Remote Sensing of Environment 225 (2019) 127–147

Contents lists available at ScienceDirect

Remote Sensing of Environment

journal homepage: www.elsevier.com/locate/rse

Current status of Landsat program, science, and applications

Michael A. Wulder[a,*], Thomas R. Loveland[b], David P. Roy[c], Christopher J. Crawford[d], Jeffrey G. Masek[e], Curtis E. Woodcock[f], Richard G. Allen[g], Martha C. Anderson[h], Alan S. Belward[i], Warren B. Cohen[j], John Dwyer[b], Angela Erb[k], Feng Gao[h], Patrick Griffiths[l], Dennis Helder[m], Txomin Hermosilla[a,n], James D. Hipple[o], Patrick Hostert[p], M. Joseph Hughes[q], Justin Huntington[r], David M. Johnson[s], Robert Kennedy[q], Ayse Kilic[t], Zhan Li[a], Leo Lymburner[u], Joel McCorkel[e], Nima Pahlevan[v,w], Theodore A. Scambos[x], Crystal Schaaf[k], John R. Schott[y], Yongwei Sheng[z], James Storey[aa], Eric Vermote[v], James Vogelmann[b], Joanne C. White[a], Randolph H. Wynne[ab], Zhe Zhu[ac,ad]

[a] Canadian Forest Service (Pacific Forestry Centre), Natural Resources Canada, 506 West Burnside Road, Victoria, British Columbia V8Z 1M5, Canada
[b] U.S. Geological Survey Earth Resources Observation and Science (EROS) Center, 47914 252nd Street, Sioux Falls, SD 57198, USA
[c] Department of Geography, Environment, & Spatial Sciences, Center for Global Change and Earth Observations, Michigan State University, USA
[d] ASRC Federal InuTeq/U.S. Geological Survey Earth Resources Observation and Science (EROS) Center, 47914 252nd Street, Sioux Falls, SD 57198, USA
[e] Biospheric Sciences Laboratory, NASA Goddard Space Flight Center, Greenbelt, MD 20771, USA
[f] Department of Earth and Environment, Boston University, MA 02215, USA
[g] University of Idaho Research and Extension Center, Kimberly, ID 83341, USA
[h] USDA, Agricultural Research Service, Hydrology and Remote Sensing Laboratory, 10300 Baltimore Avenue, Beltsville, MD 20705, USA
[i] European Commission, Joint Research Centre, Institute for Environment and Sustainability, 20133, VA, Italy
[j] USDA Forest Service, PNW Research Station, 3200 SW Jefferson Way, Corvallis, OR 97331, USA
[k] School for the Environment, University of Massachusetts Boston, 100 Morrissey Blvd, Boston, MA 02125, USA
[l] European Space Agency, Earth Observation, Science, Applications & Climate Department, Frascati (Roma), Italy
[m] College of Engineering, South Dakota State University Brookings, SD 57007, USA
[n] Integrated Remote Sensing Studio, Department of Forest Resources Management, University of British Columbia, 2424 Main Mall, Vancouver, BC V6T 1Z4, Canada
[o] United States Department of Agriculture, Risk Management Agency, Washington, DC 20250, USA
[p] Geography Department, Humboldt-Universität zu Berlin, Unter den Linden 6, 10099 Berlin, Germany
[q] College of Earth, Ocean, and Atmospheric Sciences, 104 CEOAS Admin Bldg., Oregon State University, Corvallis, OR 97331, United States
[r] Desert Research Institute, Reno, NV 89501, USA
[s] National Agricultural Statistics Service, United States Department of Agriculture, 1400 Independence Ave., SW, Washington, D.C. 20250, USA
[t] Dept. of Civil Engineering, School of Natural Resources, University of Nebraska-Lincoln, Lincoln, NE 65816, USA
[u] Geoscience Australia, GPO Box 378, Canberra, ACT 2601, Australia
[v] Terrestrial Information Systems Laboratory, NASA Goddard Space Flight Center, Greenbelt, MD 20771, USA
[w] Science Systems and Applications, Inc., Lanham, MD 20706, USA
[x] National Snow and Ice Data Center, University of Colorado, 1540 30th Street, Boulder, CO 80303, USA
[y] Rochester Institute of Technology, Chester F. Carlson Center for Imaging Science, Rochester, NY 14623, USA
[z] Department of Geography, University of California, Los Angeles, CA 90095, USA
[aa] Stinger Ghaffarian Technologies, Contractor to the U.S. Geological Survey, Earth Resources Observation and Science (EROS) Center, Sioux Falls, SD, USA
[ab] Virginia Tech, Forest Resources and Environmental Conservation, 310 West Campus Dr, Blacksburg, VA 24061, USA
[ac] Department of Geosciences, Texas Tech University, Lubbock, TX 79409-1053, USA
[ad] Department of Natural Resources and the Environment, University of Connecticut, Storrs, CT 06269, USA, United States

ARTICLE INFO

Keywords:
Open data
Remote sensing science
Land cover
OLI
TIRS
ARD

ABSTRACT

Formal planning and development of what became the first Landsat satellite commenced over 50 years ago in 1967. Now, having collected earth observation data for well over four decades since the 1972 launch of Landsat-1, the Landsat program is increasingly complex and vibrant. Critical programmatic elements are ensuring the continuity of high quality measurements for scientific and operational investigations, including ground systems, acquisition planning, data archiving and management, and provision of analysis ready data products. Free and open access to archival and new imagery has resulted in a myriad of innovative applications and novel scientific insights. The planning of future compatible satellites in the Landsat series, which maintain continuity while

* Corresponding author.
E-mail address: mike.wulder@canada.ca (M.A. Wulder).

https://doi.org/10.1016/j.rse.2019.02.015
Received 1 November 2018; Received in revised form 13 February 2019; Accepted 17 February 2019
Available online 11 March 2019

Land change science
Landsat science team

incorporating technological advancements, has resulted in an increased operational use of Landsat data. Governments and international agencies, among others, can now build an expectation of Landsat data into a given operational data stream. International programs and conventions (e.g., deforestation monitoring, climate change mitigation) are empowered by access to systematically collected and calibrated data with expected future continuity further contributing to the existing multi-decadal record. The increased breadth and depth of Landsat science and applications have accelerated following the launch of Landsat-8, with significant improvements in data quality.

Herein, we describe the programmatic developments and institutional context for the Landsat program and the unique ability of Landsat to meet the needs of national and international programs. We then present the key trends in Landsat science that underpin many of the recent scientific and application developments and follow-up with more detailed thematically organized summaries. The historical context offered by archival imagery combined with new imagery allows for the development of time series algorithms that can produce information on trends and dynamics. Landsat-8 has figured prominently in these recent developments, as has the improved understanding and calibration of historical data. Following the communication of the state of Landsat science, an outlook for future launches and envisioned programmatic developments are presented. Increased linkages between satellite programs are also made possible through an expectation of future mission continuity, such as developing a virtual constellation with Sentinel-2. Successful science and applications developments create a positive feedback loop—justifying and encouraging current and future programmatic support for Landsat.

1. Introduction

There have been dramatic changes in the Landsat program over the past ten years, many of which were made possible through actions by the two federal Landsat partners: NASA and the U.S. Geological Survey (USGS). In 2008, the Landsat data policy changed and the Landsat archive became free and open (Woodcock et al., 2008). This resulted in new paradigms for data processing and sparked a major period of innovation and understanding (Wulder et al., 2012). In February 2013, the Landsat Data Continuity Mission (LDCM) was successfully launched, since renamed Landsat-8, which adds to the archive an unprecedented number of daily acquisitions with improved geometric and radiometric properties leading to expanded scientific and operational capabilities (Loveland and Irons, 2016; Loveland and Dwyer, 2012). The increasingly long baseline of Landsat data that are geo- and radiometrically consistent and calibrated has led to the generation of new information via novel algorithmic and processing approaches. Cloud-based high-performance computing allows for bringing algorithms to data, empowering scientists and practitioners to generate new insights and robust information products over broad areas. As captured in data downloads of Landsat data, now over 1 million images per month, a large and sophisticated user base is implementing integrated analyses and often unprecedented scales (Zhe et al., 2019).

Perhaps the most objective statement on the status of the Landsat program is found in the recently released National Academies of Science Decadal Survey for Earth Science and Applications from Space (2018) assessment. We share their conclusion that:

> "The USGS has transformed the Landsat program via the Sustainable Land Imaging (SLI) program by operating Landsat, connecting the scientific/user communities and the developers of new measurement technologies, and archiving/distributing data products. This has placed the Landsat measurements on a more operational footing. As long as it is funded, and managed as an operational program, the SLI program will support and motivate widespread usage, benefitting both the operational and scientific communities."

The establishment of the NASA-USGS Sustainable Land Imaging program to ensure continuation of Landsat data collection beyond Landsat-8 allows not only science and applications but the uptake and institutionalization of Landsat measurements into programs. The determination of Landsat as an operational program with plans for a series of future launches has allowed governments to commit to the use of Landsat data to meet programmatic needs. Understanding a forward-going data stream also allows for planning and synergies among space agencies as well as national and international programs and conventions (e.g., Dolman et al., 2016; GCOS, 2016). Virtual constellations of satellites, such as between the contemporaneous Landsat-8 and Sentinel-2A and -2B satellites (Drusch et al., 2012; Loveland and Irons, 2016), allow for an effective increase in spatial and temporal coverage for both programs empowering users through increased data availability (Wulder et al., 2015). The launch of Landsat-8 maintained continuity with previous instruments while also offering improvements in the geometric and radiometric fidelity of the imagery and through the collection of approaching all possible terrestrial images on each overpass. The importance of ground systems in collecting and disseminating imagery has been demonstrated with notable benefits evident from the provision of analysis ready data products.

Ensuring Landsat continuity is the cornerstone of the program (Wulder et al., 2008; Roy et al., 2014). Major steps towards solidifying long-term continuity include the February 13, 2013 launch and subsequent mission commissioning of Landsat-8 and establishment of a Landsat-9 Architecture Study Team to define the capabilities and implementation strategy. Landsat-9 has been authorized and is proceeding towards a December 2020 launch. Planning for missions beyond Landsat-9 is also underway with the USGS defining future Landsat measurement needs (e.g., Landsat-10 and -11) and NASA initiating studies to investigate and new sensor technologies (e.g., Kampe and Good, 2017).

The 46+ year-long archive sets Landsat apart from most other satellite missions (Belward and Skøien, 2015). Substantial attention continues to be placed on expanding and improving archive holdings. The Landsat archive is expanding at an unprecedented daily rate due to the marked increase in the data acquisition rates of both Landsat-7 and -8. At present, over 1200 new images are added to the USGS Landsat archive per day (Landsat-7, ~475; Landsat-8, ~740). The expanded acquisition strategies have also increased the frequency of imaging over persistently cloudy regions of the globe and polar regions. Since the 2013 launch of Landsat-8, ~500,000 images are acquired per year, resulting in over 1 million Landsat-8 specific downloads from the USGS annually.

The Landsat Global Archive Consolidation (LGAC) initiative has continued and led to a doubling of the size of the archive with the addition of international holdings not previously part of the USGS archive (Wulder et al., 2016). A key element of mission continuity is cross-calibration across Landsat sensors. Currently, all archive holdings, from Landsat-1 through Landsat-8, adhere to a consistent radiometric framework (Markham et al., 2014; Mishra et al., 2014; Markham and Helder, 2012). Advanced processing methods and institutional capacity of the USGS was availed upon to bring Multispectral Scanner System (MSS) data from Landsats 1–5 in line with Thematic Mapper (TM) data and later Landsat instruments. This effort aims to improve the ability to conduct time series studies across the full Landsat record.

Efforts to articulate and advance a science and product vision for terrestrial global change studies (Roy et al., 2014) have led to a number of advances in data delivery, including establishment of an on-demand atmospherically collected surface reflectance product capability for all Landsat TM, Enhanced Thematic Mapper plus (ETM+), and Operational Land Imager (OLI) data (Claverie et al., 2015; Ju et al., 2012; Vermote et al., 2016), and, since 2017, implementation of a tiered collections management strategy, complemented by production of Landsat Analysis Ready Data (ARD) products for the conterminous United States (CONUS), Alaska, and Hawaii (Dwyer et al., 2018).

Based upon the convergence of programmatic, technological, and scientific events, Landsat science and applications are developing rapidly and are having a notable impact, forming links between human and earth system interactions. As described in dedicated sections later in the paper, the Landsat applications community has an increasingly large user base undertaking sophisticated, integrated, and often unprecedented analyses. The addition of Landsat-8 and the archive expansion and improvements have been particularly significant in advancing the state-of-the-art of Landsat scientific and operational applications (Roy et al., 2014). Increasing numbers of applications relate a shift to integrated large area and dense time series analyses (Wulder et al., 2018), including development of global and regional gridded composited products and derived products to understand vegetation condition, land cover change, agricultural phenomena, forest dynamics, and surface water extent, among others (Zhu, 2017). There is also an improved capacity for integrating Landsat into US Federal, other national and private sector natural resources management programs, including agricultural mapping such as yield predictions and compliance monitoring using increasingly systematic and institutionalized monitoring systems (Zhu et al., 2016; Healey et al., 2018; White et al., 2014). Utilizing Landsat thermal infrared measures for retrieval of surface temperature (Malakar et al., 2018), there has been an enhanced and improved ability to use contemporaneous thermal and solar-reflected Landsat data to derive evapotranspiration (Hendrickx et al., 2016; Anderson et al., 2012), and water use (de la Fuente-Sáiz et al., 2017; Anderson et al., 2018) information at field scales. Thermal informed application advancements have been demonstrated to improve mapping of moisture stress impacts on crop yields over large areas (e.g., Yang et al., 2018), as well as increasing the accuracy of required cloud and shadow detection and screening algorithms (Zhu et al., 2018). Of critical importance to understanding climate change, an expansion of science and applications related to cryospheric conditions and dynamics (Fahnestock et al., 2016) has also taken place. There is an increasing clear understanding of the supporting mechanisms and the benefits of synergies among space agencies. Virtual Constellations of satellites, such as between Landsat-8 and Sentinel-2 (Wulder et al., 2015), allow for an effective increase in spatial and temporal coverage (Li and Roy, 2017), empowering users through increased data availability.

Building upon the insights and experiences of the 2012–2017 USGS/NASA Landsat Science team as well as the research context communicated by Roy et al. (2014), the aim of this article is to support and elaborate on recent progress of the Landsat program and the science and applications that are being enabled. Above we highlighted key elements and recent Landsat program achievements; in the following sections we support and elaborate more fully on these topics. We highlight the programmatic and policy advances that have led the Landsat program to the point where it has achieved long-sought programmatic stability, improved technical capability, and expanded scientific and operational applications. We also describe with examples the context and recent trends that may further advance Landsat science and applications, and conclude with an outlook of the future including consideration of interoperability with the Sentinel-2 constellation and the planned Landsat-9 and -10 systems.

2. Programmatic developments

2.1. Continuity

Landsat mission continuity is supported by the 1992 US Land Remote Sensing Act which maintains that the US Government should ensure a permanent, global Landsat imaging archive to enable long-term monitoring of Earth's changing land surface and climate, both natural and human-induced (Wulder et al., 2008). Landsat continuity is defined by systematic 16-day global, imaging coverage of continents, islands, corals, and coastal oceans, no-cost access to the entire image data archive, and adherence to comparable temporal, spatial, spectral, and radiometric measurements.[1] The traceable radiometric and geometric accuracy and stability standards of Landsats 1–8 is unparalleled (Markham and Helder, 2012; Markham et al., 2014; Mishra et al., 2014), and Landsat is distinguished by being both the first medium resolution Earth observation satellite as well as the longest running continuous program (Belward and Skøien, 2015). For most of Landsat's history, there have been two satellites in orbit providing 8-day temporal repeat around which governments, scientists, businesses, and data users at-large have developed infrastructures and investments assuming an uninterrupted data stream.

Given over 50 years of planning and operations, the Landsat program is multifaceted and highly complex. A comprehensive history of the Landsat program can be found in Goward et al. (2017). As shared in Fig. 1, each Landsat mission can be considered by Mission Acquisition (i.e., planning, financing, building, pre-launch activity) and Mission Operations comprising data and related management activities (e.g., image scheduling, downlink, archiving, dissemination). Mission Acquisition has largely been the purview of NASA, with responsibilities currently divided between NASA (space segment) and USGS (ground segment). For Landsat-4 and -5 Mission Operations were made a commercial responsibility under a contract to NOAA (National Oceanic and Atmospheric Administration) which also coincided with similar commercial responsibilities for Data Distribution and Archiving. Since 2001, both data distribution and archiving have been the responsibility of the USGS. Mission Acquisition for the Earth Resources Technology Satellite (ERTS; later renamed Landsat-1) was initiated by NASA in 1967 leading to a July 23, 1972 launch (Goward et al., 2017). Since that time, there has always been at least one Landsat satellite in orbit and collecting data (Wulder et al., 2008). The notable 29-year longevity of Landsat-5 (with a 3-year design life) mitigated the failure of Landsat-6 to reach orbit.

Landsat sensors have developed from initially having four broad bands, to having increasingly narrow, numerous, and well-positioned wavelength ranges (Fig. 2). The initial Landsat-1 Multispectral Scanner System (MSS) launched in 1972 had spectral bands that occupied visible and near infrared wavelengths and were collecting data that was typically resampled to 60-m at a 6-bit quantization—a sensor configuration that was repeated for MSS onboard the subsequent Landsats-2 and -3. With the Thematic Mapper (TM) on Landsat-4 and -5, the number of spectral bands increased to seven at 8-bit quantization. The six optical bandpasses were positioned differently than the MSS and the six optical channels had a spatial resolution of 30 m. Notably, TM saw the introduction of two shortwave infrared (SWIR) channels. The Enhanced Thematic Mapper Plus (ETM+) onboard Landsat-7, had largely similar spectral and spatial resolution characteristics as the TM, with the exception of an additional 15-m spatial resolution panchromatic channel and a 60 m TIR band instead of the 120 m spatial resolution of TIR and Landsat-4 and -5. The Operational Land Imager (OLI) on Landsat-8 furthered the previous trend of refined spectral band passes and the addition of new channels, now with 12-bit quantization. OLI

[1] https://landsat.usgs.gov/sites/default/files/documents/LST_Landsat_Continuity_Requirements.pdf [accessed: February 22, 2019].

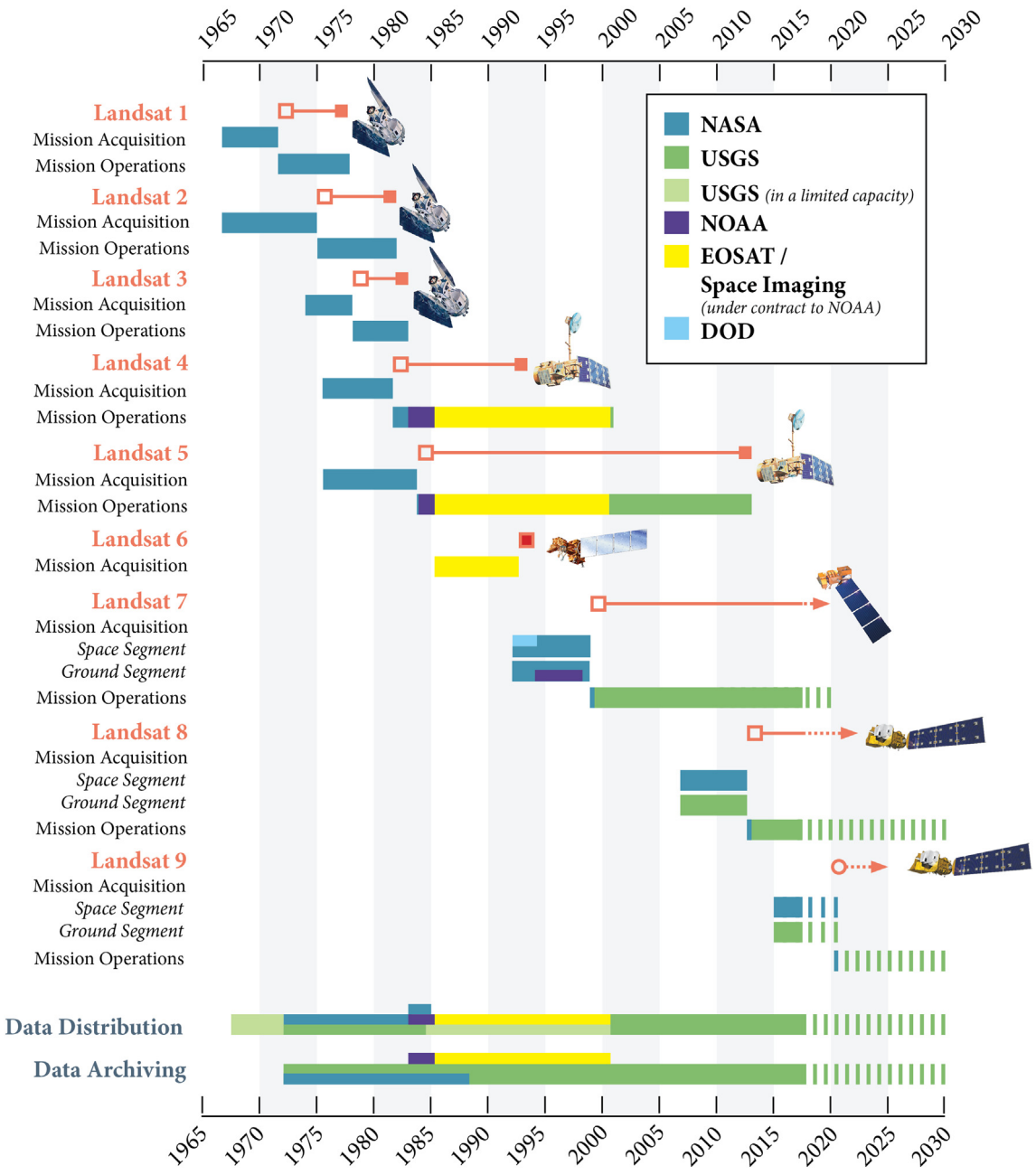

Fig. 1. Landsat mission series and management history. Six decades of program management responsibilities. The broken bars relate anticipated future management plans. For additional detail see Goward et al. (2017). (Source: NASA/Landsat Legacy Project Team and American Society for Photogrammetry and Remote Sensing).

has an enhanced blue (coastal aerosol) and cirrus channel to inform aquatic science and applications and to improve cloud detection and screening, respectively. The backwards compatibility of OLI with prior instruments, coupled with OLI's substantially improved radiometry (Irons et al., 2012; Schott et al., 2016), have greatly expanded Landsat science and applications in cryosphere and aquatic science areas in particular. Beyond the spatial, spectral, and radiometric characteristics noted above, the satellites, detectors, communications, downlink capacity, and ground system technology have likewise advanced and changed over time.

Landsat's continuity is especially important because it provides a unique medium long thermal infrared measurement record that began in 1982 with Landsat-4 (Schott et al., 2012). As spectral response functions and 60 to 120-meter spatial resolution varied between Landsat instruments over time, considerable effort has been undertaken to ensure radiometric consistency among the sensors (Schott et al., 2012). The Thermal Infrared Sensor (TIRS) aboard Landsat-8 experienced stray light problems early in the mission (Montanaro et al., 2015) and technical adjustments to the TIRS have stabilized its measurement performance on orbit (Montanaro et al., 2014; Schott et al., 2014). In addition to its important value for systematic cloud screening, the full potential of Landsat's thermal infrared record will be more fully realized once atmospheric compensation algorithms to retrieve surface temperature reach an operational production phase (e.g., Malakar et al., 2018).

Because Landsat's measurement continuity is traceable and of high quality, mission science objectives can be maintained throughout the entire image archive to the pixel-level (NRC, 2013). Furthermore, the measurement record is characterized by systematic spatial and temporal uncertainty and repeatability metrics all the way through to data processing systems and distribution. More broadly, continuity of Landsat's calibrated measurements ensures scientific integrity and

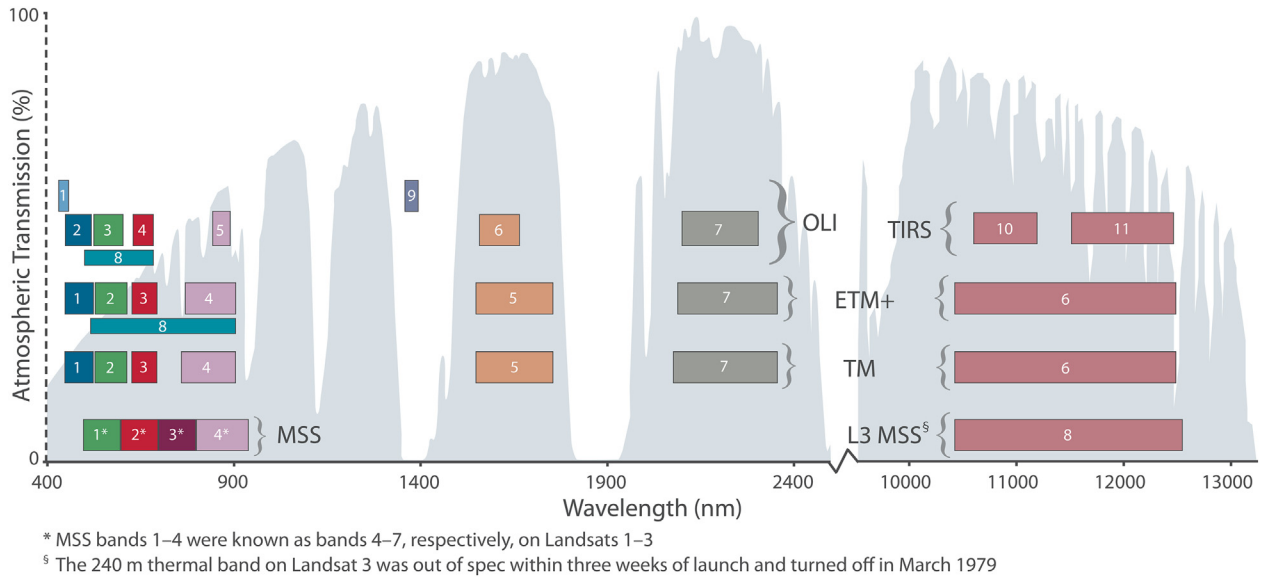

Fig. 2. Landsat sensors, spectral channels and band-passes, superimposed on atmospheric transmission percentage (grey background). MSS: Landsat-1 through -5; TM: Landsat-4 and -5; ETM+: Landsat-7; OLI and TIRS: Landsat-8. (Source: NASA/Landsat Legacy Project Team and American Society for Photogrammetry and Remote Sensing).

objectivity for climate science and global change research. Table 1 outlines Landsat continuity characteristics and the specifics which enable a reliable data stream. It is important to note from the description above that measurement continuity encompasses both space and ground segments, with data delivery and science supported products as key elements. These elements identified in Table 1 are essentially minimums to enable continuity, with the incorporation of new technology and exceeding these elements (as noted previously with changes to spatial, spectral, and radiometric characteristics) being possible and desirable.

2.2. Landsat products and processing

In recognition of the need for improved usability and consistency among Landsat sensors, the global Landsat-1 to −8 archive was reprocessed as Collection 1 with reprocessing finished May 2017 (Dwyer et al., 2018). The Collection 1 data are now the standard available data (https://landsat.usgs.gov/landsat-collections; [accessed: Jan 10, 2019]). Provision of Landsat data with consistent geometric and calibrated radiometric qualities supported by metadata and per-pixel quality flags enables data users to focus time on analysis rather than preparing for analysis. To further reduce the pre-processing burden on users, Landsat ARD products were generated using the Collection 1 algorithms. ARD products are available for search and download over the conterminous United States (CONUS), Alaska, and Hawaii for Landsat-4, -5, -7 and -8 (Dwyer et al., 2018). ARD are provided as tiled, top of atmosphere and atmospherically corrected products defined in a common equal area projection, accompanied by spatially explicit quality assessment information, and appropriate metadata to enable further processing while retaining traceability of data provenance (Dwyer et al., 2018). Planning is underway to extent the ARD products to Landsat-1 to -5 MSS data and global ARD production is being considered. The readiness for automated processing is predicated on three key ideas: geometric alignment (stackability), radiometric consistency including atmospheric correction, and metadata and per-pixel quality information. This ensures that all images are processed in a consistent manner that is anchored by traceability standards and calculations that follow the pixel data from the instrument level to the user.

2.2.1. Geometric alignment

At the most fundamental level, observations of the Earth's surface need to be both geometrically aligned with known geometric accuracy based on a dense network of ground control locations. Precise and accurate alignment within (band-to-band) and between (sensor-to-sensor) multiple earth observation datasets is required to enable integration with other spatial datasets, and is, most importantly, a precursor to change detection and time series analyses. This is especially important for analysis ready data intended for automated processing, because many hundreds to thousands of scenes can be analysed in a single run, without any visual review of individual images. Slight misregistration can result in noisy time series, especially for locations that have sharp surface discontinuities, such as the edge of a field. Larger misregistration errors can result in unacceptable classification errors. To mitigate this risk, the USGS has stratified the Collection 1 data into Tier 1 and

Table 1
Landsat continuity characteristics and specifications (elements after Wulder et al., 2008).

Element	Description
Data accessibility	Systematic data archive, non-discriminatory distribution, free
Geographic coverage	Landmasses, coastal oceans, ice sheets, islands, and coral reefs
Temporal frequency	Single mission 16-day revisit; 8-day revisit with two satellites (sun-synchronous orbit)
Spectral bands	Visible, near-infrared, shortwave-infrared, thermal infrared
Spatial resolution	30 to 60-m solar reflective; 60 to 120-m thermal infrared
Radiometric calibration accuracy and stability	Within 5% absolute spectral radiance; within 3% top-of-atmosphere reflectance; within 2% thermal infrared spectral radiance
Radiometric performance	Meet or exceed Landsat-8 performance (i.e., 12 bits with signal-to-noise and noise-equivalent-change-in-temperature for the reflective and thermal wavelength bands (Irons et al., 2012))
Geometric and geodetic accuracy	Tier 1 ≦ 12-meter radial RMSE

Tier 2 categories based on the geometric accuracy of the imagery (Tier 1 data have geodetic accuracy with ≦12-m Root Mean Square Error (RMSE), and Tier 2 data have accuracy > 12-m) giving users a level of certainty with respect to geometric accuracy when performing automated analysis (https://landsat.usgs.gov/what-are-landsat-collection-1-tiers; [accessed: Jan 10, 2019]).

Improving satellite navigation technologies (e.g., global positioning system (GPS), high precision star trackers, inertial measurement devices) over the span of the Landsat missions have enabled improvements in the inherent (pre-adjusted) geolocation accuracy of Landsat products from kilometers for Landsat-1 to -3, to hundreds of meters for Landsat-4 through -7, to tens of meters for Landsat-8. The geolocation accuracy of Landsat-8, benefitting from recent technological advances, at 18 m 90% circular error (Storey et al., 2014), is essentially equivalent in accuracy to the Global Land Survey (GLS) ground control point network that is used to geometrically correct Landsat products from all missions. This inherent accuracy enhances the utility of scenes where the application of ground control points is impractical due to cloud cover, lack of surface features (e.g., ice sheets), or instability of the surface features (e.g., dune fields) (Roy et al., 2014).

Historically, alignment of the global Landsat archive with the Earth's surface has been achieved through Global Land Survey ground control point chip sets (Gutman et al., 2013). The inclusion of a fully operational GPS on Landsat-8 has made it apparent that the absolute geometric accuracy of the Landsat archive needed to be improved through a re-baselining of the geometric ground control to a more recent chip set. Currently, the Landsat chip set is being readjusted to be consistent with the Sentinel-2 Global Reference Image (Dechoz et al., 2015) and the Collection 1 data will be reprocessed as Collection 2 (Storey et al., 2016). Aligning the global Landsat archive with the Sentinel-2 global reference image will ensure that the Landsat archive is aligned to (a) the Earth's surface, (b) other Landsat observations, and (c) other EO observations such as those acquired by the Sentinel series of sensors. Landsat-8 data have been used to reposition the GLS control points in regions where the GLS control points are least accurate, thereby improving the absolute positional accuracy of data products throughout the Landsat archive (Storey et al., 2014).

2.2.2. Radiometric comparability and surface reflectance

The Landsat archive is well calibrated and is referenced to the most accurate instrument in the series, Landsat-8 OLI (Mishra et al., 2014). Along with sensor and operational improvements, radiometric calibration accuracy has improved from ~10% in the era of Landsat-1 to 3% with Landsat-8 (Markham et al., 2014; Morfitt et al., 2015). In Collection 1, a reflectance-based calibration is used as it has higher accuracy than previous radiance-based calibration approaches. The Landsat-8 calibration is propagated to earlier sensors using data sets from adjacent Landsat sensors acquired during near-simultaneous nadir overpasses. Each Landsat sensor in the series temporally overlapped the preceding sensor and the following sensor. During these overlap periods, select data sets were measured over stable test sites to provide a calibration transfer between these data sets. Implementation of this cross-calibration has been completed for Landsats 1–8 and is maintained as post-launch cal/val responsibility at USGS EROS.

Atmospheric effects can have a considerable impact on Landsat data. Whilst some analyses that are robust to radiometric precision and accuracy can be performed on 'top of atmosphere' (TOA) reflectance products (Song et al., 2001), an increasing number of analytical techniques, especially those that make use of time series analysis (Zhu and Woodcock, 2014a) or multi-temporal composites, rely on the availability of surface reflectance (Hermosilla et al., 2015a). Atmospheric correction over land, even if imperfect, is needed as input for higher-level surface geophysical parameter derivation and products (Justice et al., 1998). It is also often necessary to use the surface reflectance product in multitemporal or multispectral image-based applications aimed at detecting and monitoring changes on the Earth's surface (e.g., anthropogenic impacts) (Vermote et al., 2002). Atmospheric corrections over aquatic systems are particularly critical for the retrieval of water quality products (e.g., concentrations of total suspended solids, chlorophyll, and dissolved organic carbon) and to enable reliable time series analyses of water resources and aquatic ecosystems (Gordon, 1997; Pahlevan et al., 2018).

Based on the increasing number of analyses that rely on surface reflectance as input, surface reflectance is increasingly understood as a minimum standard for analysis ready data. Additional corrections for satellite view angle and terrain illumination effects can also be implemented (Lewis et al., 2017; Roy et al., 2016a). Atmospheric correction relies on the modeling of the coupled surface-atmosphere system (radiative transfer) (Vermote et al., 1997) and the assumption the data are calibrated to the absolute standard (reflectance). For Landsat, the differences between top of atmosphere reflectance and surface reflectance over most land surfaces are more pronounced in the visible range (blue to red) and typically reach 0.02 (red)–0.04 (green) reflectance unit over vegetation, which is of the same magnitude as the surface signal (Ju et al., 2012). Over turbid or eutrophic inland or nearshore coastal waters, a greater portion of at-sensor signal arises from atmospheric scattering and absorption (i.e., > 90% in the blue bands) (Gordon and Wang, 1994; Pahlevan et al., 2014a) and atmospheric correction is particularly needed.

At the time of this writing, multiple atmospheric correction algorithms have been proposed and USGS EROS has implemented two of them for Landsat-8 (Landsat Surface Reflectance Code, LaSRC) (Vermote et al., 2016) and Landsat-4, -5, and -7 (Landsat Ecosystem Disturbance Adaptive Processing System, LEDAPS) (Masek et al., 2006) data. The uncertainty of the atmospheric correction is on the order of 5–10% depending on spectral channel and underlying atmospheric conditions. Coupling this with a Landsat-8 3% radiometric calibration uncertainty increases the uncertainty of a surface reflectance product to the range of 6—10% (Vermote et al., 2016). Characterization of the quality of surface reflectance means that in addition to the established methods for evaluating on-orbit calibration precision (Chander et al., 2009), there is a need to quantify the radiometric accuracy of surface reflectance products (Pahlevan et al., 2014b; Vermote et al., 2016). The absolute radiometric accuracy of surface reflectance products is underpinned by the need for a systematic comparison of satellite-derived surface reflectance values with in-situ surface reflectance measurements (Doxani et al., 2018). For example, the Land Product Characterization System has been established to enable comparative analysis of satellite and in-situ surface reflectance measurements (Gallo et al., 2017).

An additional element of ensuring that data is 'analysis ready' is providing access to the relative spectral responses of the specific sensors. For example, the Landsat-8 OLI and Sentinel-2 MSI spectral response functions are described in Barsi et al. (2014a) and Gascon et al. (2017). Some authors have developed sensor specific models that account for the way in which specific absorption features interact with the relative spectral response of each sensor (Lymburner et al., 2016). Others have developed statistical calibration factors to adjust the spectral reflectance of similar sensor bands (Roy et al., 2016b; Zhang et al., 2018). This is especially important in an era when time series and temporal change detection analyses are increasingly being constructed from observations from more than one sensor.

2.2.3. Collection and granule level metadata and per-pixel quality assurance information

Collection (overall dataset) and granule (image specific) level metadata (as described at https://earthdata.nasa.gov/about/science-system-description/eosdis-components/common-metadata-repository/unified-metadata-model-umm; [accessed: Jan 10, 2019]) are required to ensure traceability of products generated from collections (Lewis et al., 2017). This traceability enables granules to be linked to other contexts (such as with point data or data from other sensors), and to

allow searching of the data archive. The ability to include or exclude observations that are affected by cloud (or related cloud shadow) is essential for automated processing of large volumes of data and in the generation of time series. The generation and utilization of per pixel 'QA' band information is already well established within the MODIS community (Roy et al., 2002). This level of per-pixel quality assurance information allows for exclusion of observations affected by sensor factors such as 'no data' (for example scene edges and 'scan line correction off' gaps, sensor saturation, and non-contiguous observations). Per-pixel QA band information is also required to exclude cloud and cloud shadow affected observations. The performance of ARD can be further enhanced by a shift from sensor specific formats such as path/rows to a sensor agnostic tiling system that includes self-contained metadata within the file format and deployment of these files on high-performance computing infrastructure.

3. Trends in analytical approaches

3.1. Time series

Tracking change through time has always been central to the Landsat mission, and recent years have seen a revolution in time series techniques that take full advantage of Landsat's unique historical record to monitor change (Zhu, 2017). Coupled with increasingly affordable computation as well as automated atmospheric correction algorithms (Masek et al., 2006) and cloud detection algorithms (Zhu and Woodcock, 2012), temporally-dense analysis has been increasingly applied over large areas and in diverse thematic domains. Moreover, by considering the spectral history of each footprint on the ground as a time series, more nuanced understanding of the changes on the Earth's surface has been possible.

Temporally dense, per-pixel analysis has been parlayed into a wide variety of science and application products. Foundational image datasets built on Landsat best-pixel composites (Griffiths et al., 2013a; Roy et al., 2010; White et al., 2014) have allowed subsequent development of applied maps of condition and change (Gómez et al., 2012; Hansen et al., 2014; Hermosilla et al., 2015a, 2015b; Schroeder et al., 2011; White et al., 2011; White et al., 2014; Yan and Roy, 2014, 2016; Griffiths et al., 2018; Roy and Yan, 2018). Algorithms that focus directly on disturbance have also benefited from the temporally-dense Landsat data (Brooks et al., 2012; Huang et al., 2010; Hughes et al., 2017; Kennedy et al., 2010; Zhu et al., 2012), allowing investigation of drivers of change (Alonzo et al., 2016; Pahlevan et al., 2018), national to global-scale assessment of disturbance (Hansen et al., 2013;

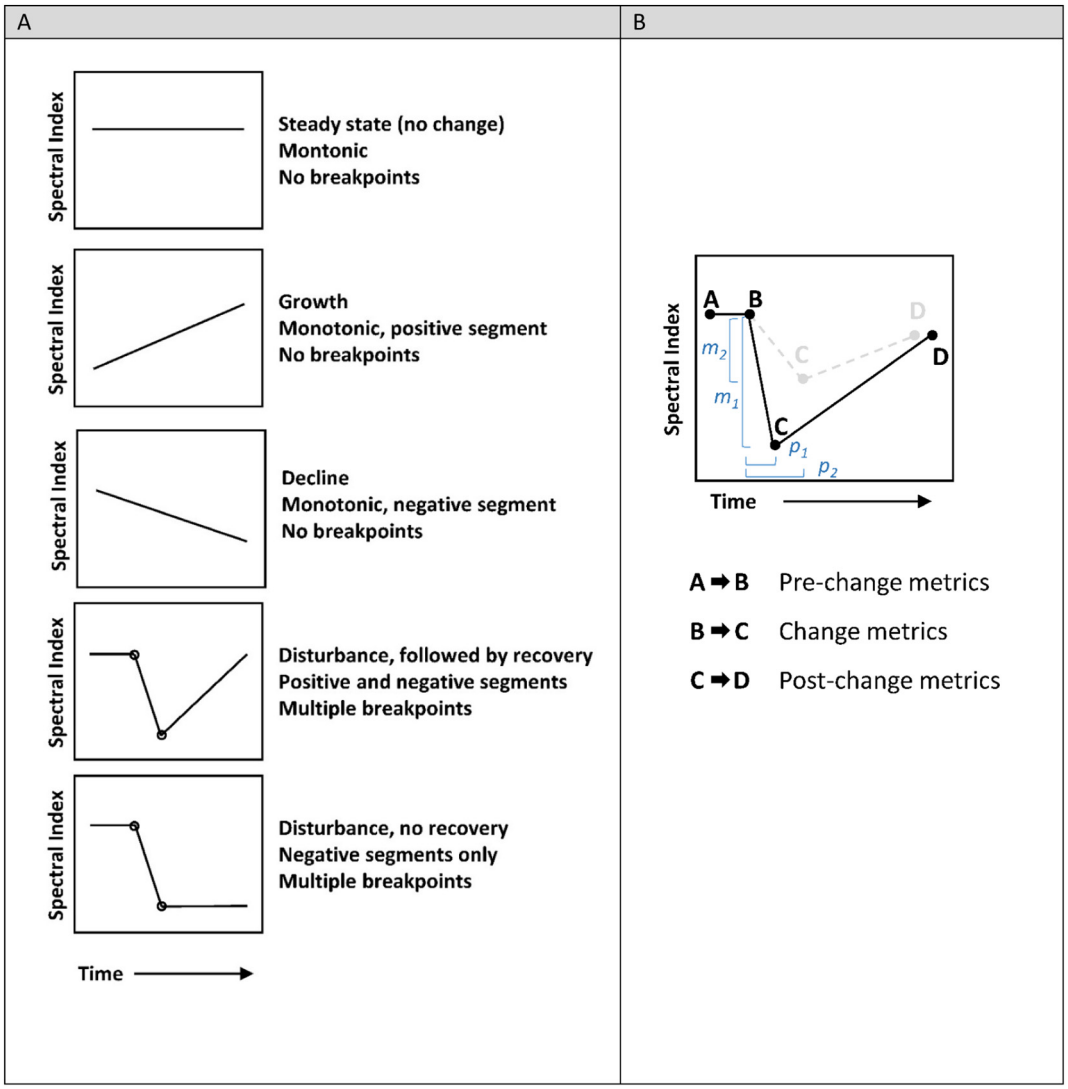

Fig. 3. Panel A. Example Landsat time series trajectories for different forest states and their characteristics (after Meigs et al., 2011 and Pflugmacher et al., 2012). Panel B. A graphical representation of Landsat time series change metrics. Different disturbance types will have different metric values (e.g., different change magnitudes (m_1 versus m_2) and persistances (p_1 versus p_2)).

Hawbaker et al., 2017; Masek et al., 2013; Griffiths et al., 2018) that themselves can play into improved modeled estimates of change (Williams et al., 2016). More broadly, dense time series of Landsat data are eminently suitable for detection of land cover change, including for urban areas (Schneider, 2012), agricultural regions (Hurni et al., 2017; Yan and Roy, 2016; Roy and Yan, 2018), and water dynamics at the global scale (Pekel et al., 2016). Reviews of recent algorithm development and change products are available in Zhu (2017), Wulder et al. (2012), and Wulder et al. (2018).

Building on the analysis of temporally dense Landsat data, time series approaches leverage the entire temporal domain to understand a wide range of changes on the Earth's surface. In this paradigm, the spectral trace of a given pixel can be considered an ecological response curve whose shape reveals something about the underlying processes causing the change (Kennedy et al., 2014). Increasingly researchers fit regression lines and splines to sequences of Landsat images (Hostert et al., 2003; Lawrence and Ripple, 1999). Such time series algorithms allow detection of long, slow evolution in landscapes, including those caused by degradation and by growth (Goodwin et al., 2010; Meigs et al., 2011; Senf et al., 2015; Vogelmann et al., 2012; White et al., 2017), as well as cyclical processes related to phenology (Melaas et al., 2016; Pasquarella et al., 2016) and crop development and harvesting (Gao et al., 2017; Roy and Yan, 2018). Such conceptualization of land surface change extends beyond automated approaches to the tools used to interpret and validate maps of change (Cohen et al., 2010), which in turn can provide statistical insight into causes of change at national scales (Cohen et al., 2016; White et al., 2017; Hermosilla et al., 2015b, 2016).

Underpinning the aforementioned advances in monitoring with Landsat time series are temporal spectral metrics. These metrics characterize temporal trends through time, distilling complex change trajectories (Fig. 3, Panel A), and providing continuous variables that can support an array of modeling applications. Metrics are generated from the seasonal and annual trends, segments, and breakpoints of the temporal analysis of the time series and characterize the change event, as well as pre- and post-change conditions (Fig. 3, Panel B). As evident in Fig. 3, time series metrics can capture and describe variable lengths of time, dictated by the characteristics of the trends found in the time series. Landsat time series metrics are essential for attribution of disturbance types (Hermosilla et al., 2015b; Kennedy et al., 2015; Moisen et al., 2016; Schroeder et al., 2017) and land cover classes (Gómez et al., 2016; Hermosilla et al., 2018). Metrics characterizing post-change conditions have been used to characterize both the short- and long-term return of vegetation post-disturbance (Kennedy et al., 2012; Griffiths et al., 2014; White et al., 2017). Pflugmacher et al. (2012) used Landsat time series metrics to significantly improve predictions of biomass, basal area, and Lorey's mean height, and subsequent studies have demonstrated that the longer the time series, the greater the increase in prediction accuracy (Pflugmacher et al., 2014; Bolton et al., 2018).

3.2. Pixel-based processing

Landsat imagery are increasingly used for large area characterizations of land surface processes and temporal image compositing approaches have been instrumental for this. Transitioning from scene-centered (e.g., cloud free scenes) Landsat data analysis towards a pixel-based (e.g., cloud free pixels) processing perspective was fundamental for enabling compositing with Landsat data (Kennedy et al., 2014). The requirements for this were satisfied through important developments such as the open data policy, improved geometric quality of Landsat data, ubiquitous IT resources and fully automated algorithms for atmospheric correction (Schmidt et al., 2013; Vermote et al., 2016) as well as cloud/cloud-shadow masking (Zhu and Woodcock, 2012; Zhu and Woodcock, 2014b). This has enabled users of Landsat data to transform segments of the Landsat archive into viable data that can be exploited in large-area processing approaches.

From an algorithm perspective, most compositing approaches applied to Landsat data follow a best-pixel selection strategy, often using simple selection criteria such the maximum NDVI or median NIR (Potapov et al., 2011) or consider multi-band distributions of cloud-free candidate observations (Roy et al., 2010; Flood, 2013). Other best-pixel approaches additionally consider similarity criteria (Nelson and Steinwand, 2015) or derive a decision through a weighted evaluation of several image and scene based parameters (Griffiths et al., 2013a; White et al., 2014; Frantz et al., 2017; Griffiths et al., 2018). Contrary to best-pixel selection approaches, some approaches calculate new spectral values such as in mean-value compositing (Vancutsem et al., 2007) or generate synthetic images based on harmonic time series fits (Zhu et al., 2015a).

Applications that utilize compositing for large area Landsat analyses frequently target forest cover and forest change analyses. Integration of multi-year imagery has enabled the mapping of the entire boreal forests and related changes (Potapov et al., 2011), forest dynamics in Eastern Europe in the context of socio-economic transitions (Griffiths et al., 2014; Potapov et al., 2015). Sub-continental assessments of annual forest cover changes and the attribution of change agents have been performed for all of Canada (White et al., 2014; Hermosilla et al., 2016). The first global assessments of forest cover and disturbance was performed with Landsat data building heavily on distributed cloud-computing and a suite of composites and other metrics (Hansen et al., 2013; Gorelick et al., 2017). Agricultural applications based on large-area Landsat compositing include multi-decadal compositing for disentangling grassland-cropland dynamics in Eastern Europe (Griffiths et al., 2013b). Anomaly mapping based on multi-decadal compositing and differencing of NDVI has proven useful for monitoring agricultural drought and groundwater dependent ecosystems in the Great Basin, USA (Huntington et al., 2016, 2017).

4. Science and application advances

The following sub-sections present a synthesis of the state-of-the-art for recent Landsat related science and applications.

4.1. Application areas

4.1.1. Cryosphere

Landsat-8 has transformed snow and ice research, having a far greater impact on this field than any of the earlier Landsat series satellites. New products and research paths have built upon the Landsat programs' initial potential for mapping and characterizing unknown areas of the polar regions, first recognized soon after Landsat-1 (e.g., Swithinbank, 1988; Williams and Ferrigno, 2010) and developed further with Landsat TM (e.g., Hall et al., 1987; Orheim and Lucchitta, 1987; Orheim and Lucchitta, 1988; Steffen and Schweiger, 1991; Scambos et al., 1992). The improvement in applicability to cryospheric research stems from three advances in the Landsat-8 Operational Land Imager (OLI) and post-acquisition processing: increased radiometric resolution (to 12-bit), with a concurrent adjustment of the visible – near-infrared dynamic range; improved geolocation accuracy to < 1 pixel ground-equivalent scale; and an increase in image acquisition rate (now > 700 scenes/day). With polar overlap of the scenes, polar glaciers, ice sheets, and the peripheral sea ice along the Arctic and Antarctic coastal areas are observed on a sub-monthly basis (cloud cover permitting). Landsat-8's off-nadir viewing capability has permitted new first-time Landsat program image acquisitions at up to 84° latitude. Landsat-8 TIRS has proven useful both for low-temperature mapping of the central Antarctic ice surface (Fogt and Scambos, 2014; Scambos et al., 2018) and debris cover mapping on glaciers (Bhardwaj et al., 2015), despite early issues with stray light and detector array calibration (Barsi et al., 2014b; Montanaro et al., 2014). Polar application of the TIRS sensor is now aimed at tracking details of ocean surface

temperature at tidewater glacier fronts and icy fjords (similar to past work using Landsat-7; Mankoff et al., 2012).

Perhaps the most significant improvement from Landsat-8 for glaciological science has been in mapping ice flow velocity in glaciers and ice sheets (e.g., Jeong and Howat, 2015; Fahnestock et al., 2016; Mouginot et al., 2017). The improvement in radiometric sensitivity has resulted in a new capability of mapping smooth unfractured ice sheet regions on the basis of snow surface texture alone (demonstrated in Bindschadler, 2003), greatly extending the mappable area of the ice sheets. Improved geolocation and high acquisition rates are supporting a finer temporal resolution for ice flow change detection, which has revealed far larger ranges in ice flow, both seasonally and interannually, than had been appreciated previously (Fig. 4). Landsat data enables near-real-time monitoring and communication of glacier and ice sheet velocity (e.g., https://nsidc.org/data/golive; [accessed Jan 10, 2019]). Improved radiometry in the visible bands of Landsat-8 also greatly improved the mapping of meltwater lakes on the ice sheets (e.g., Pope et al., 2016; Miles et al., 2017; Kingslake et al., 2017). High acquisition rates support near-weekly monitoring of lake formation, drainage, and freeze-up dates, which in turn provides greater detail for studies of glacier acceleration in response to lake drainage to the base of the ice sheet.

Landsat has been used widely to map snow cover extent (Crawford et al., 2013; Dozier, 1989), subpixel fractional snow cover (Rosenthal and Dozier, 1996), and snowmelt timing (Hall et al., 2015). Landsat has also served as an essential medium resolution reference source for validation of snow mapping algorithms for MODIS snow products (Rittger et al., 2013). Despite Landsat's valuable role for snow remote sensing science, further advancements will have to overcome several remaining challenges that include accurate cloud and cloud shadow detection and screening over snow and ice surfaces (Choi and Bindschadler, 2004; Crawford, 2015), mapping snow underneath dense forest (Klein et al., 1998), low solar zenith illumination angles in winter, removal of aerosol effects during atmospheric compensation processing, and increased temporal revisit frequency to enable tracking of persistent snow cover at regional scales and beyond (Crawford, 2015; Selkowitz and Forster, 2016).

4.1.2. Aquatic science and surface water mapping

The notably improved signal-to-noise (SNR) performance of OLI (Morfitt et al., 2015) plus the addition of the coastal aerosol band have dramatically improved Landsat-8's ability to map water quality. The Landsat TM and ETM+ instruments have traditionally been used to monitor turbidity in fresh and coastal waters and, if the turbidity was only a function of a single parameter, potentially map that parameter (Kloiber et al., 2002). Gerace et al. (2013) and Pahlevan and Schott (2013) predicted that the increased SNR expected from OLI's push-broom design as well as the new 443-nm band can potentially improve

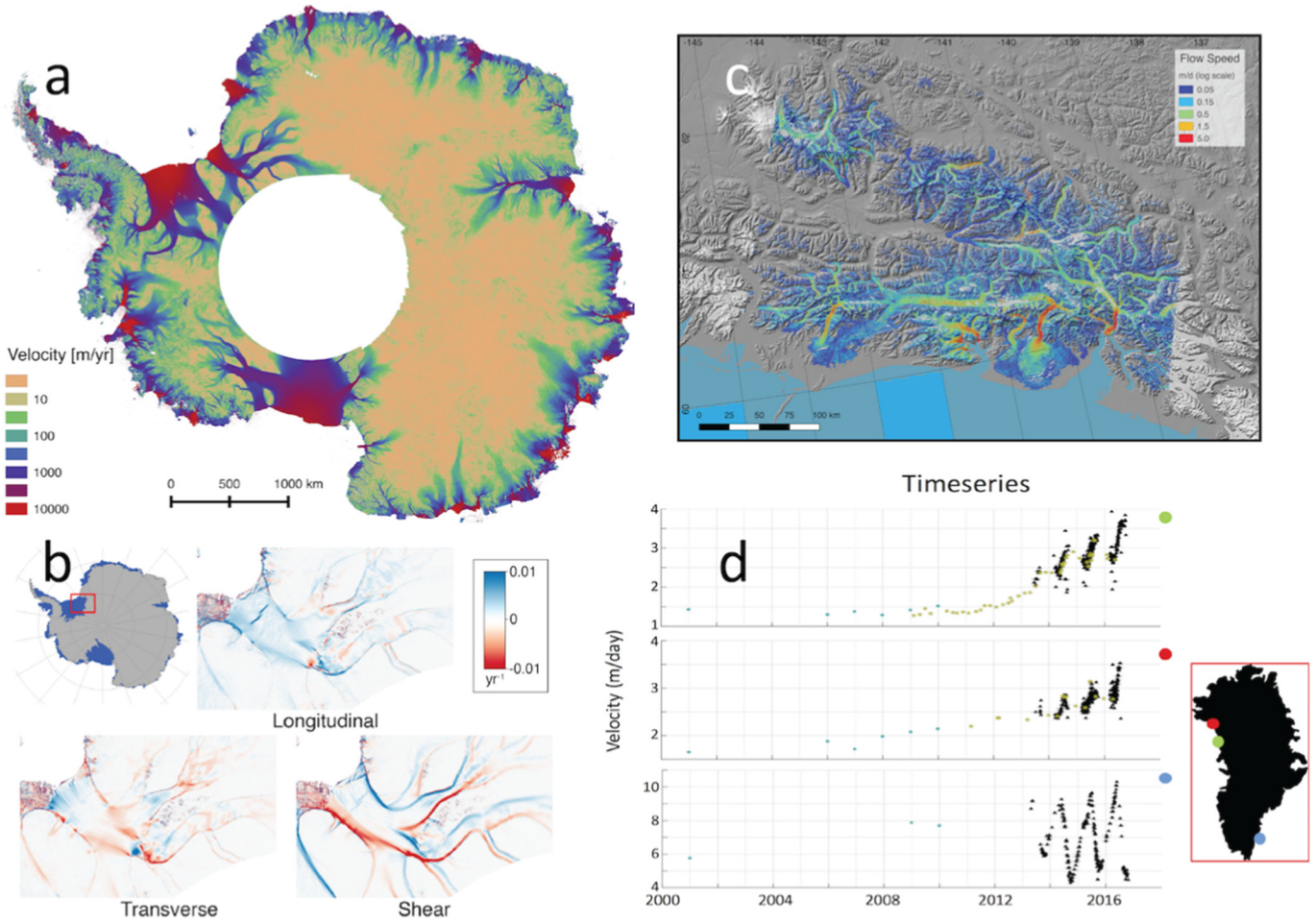

Fig. 4. Examples of ice sheet and glacier velocity mapping and derived products using Landsat-8. a) Landsat Ice Speed Map of Antarctica (LISA; NSIDC data set, www.nsidc.org [accessed February 22, 2019]; Gardner et al., 2018); b) ice surface strain rate maps of the Slessor and Recovery glaciers based on the LISA mapping (Alley et al., 2018); c) ice speed map of southeastern Alaska glaciers, spanning 2013–2015 data (Fahnestock et al., 2016); d) time series of three glacier outlets (centerline, near the grounding line) showing the increase in flow speed and the ability to measure seasonal change with the high frequency of coverage of polar areas. In the graph, small blue and green dots are ice flow speeds from InSAR satellites (Radarsat and TerraSAR-X) and black dots are Landsat-8 image pair–derived speeds. (For interpretation of the references to color in this figure legend, the reader is referred to the web version of this article.)

simultaneous quantitative retrieval of the three primary coloring agents in fresh and coastal waters (chlorophyll (Chl), total suspended solids (TSS) and yellowing organics (colored dissolved organic materials (CDOM)). Drawing on OLI's on-orbit SNR (Pahlevan et al., 2014b) which significantly exceeded requirements (and exceeds TM/ETM+ performance by up to a factor of eight). Concha and Schott (2016) demonstrated that this potential was achieved. The low SNR of heritage Landsat instruments had previously restricted the utility of empirical algorithms (e.g., band ratio) sensitive to random/systematic noise. Not only water quality mapping but also bottom composition mapping (e.g., coral reefs) in optically shallow waters are significantly enhanced (e.g., Hedley et al., 2018; Wei et al., 2018). High-fidelity retrievals of water quality parameters or bottom composition is contingent upon a robust processing method for the removal of atmospheric effects, of which, aerosol contributions are the most variable in space and time. The heritage ocean color processing system (Franz et al., 2015) has proven to perform well in moderately turbid nearshore coastal waters (Pahlevan et al., 2017) allowing for time series analyses of global coastal waters as well as complex biogeochemical cycling in land-water interface. It is only with a rigorous atmospheric correction that the aquatic community is able to devise algorithms for the retrievals of TSS and Chl, which requires a vast amount of collocated field radiometric data. A widely used ocean Chl algorithm using a blue-green ratio has been demonstrated to provide reasonable products over moderately eutrophic coastal waters (Franz et al., 2015; Pahlevan et al., 2016). However, due to the empirical nature of these algorithms (Lymburner et al., 2016; Nechad et al., 2010) and the complex optical regime in inland and nearshore coastal waters, algorithms are often region-specific, necessitating parameter tuning.

The cumulative inference indicates an enormous advance for the aquatic community. Until now, quantitative multi-constituent retrieval of water quality parameters had largely been restricted to ocean color missions like MODIS and SeaWiFS. Evaluating water quality in spatially heterogenous inland and nearshore coastal waters (bays, harbors, etc.) was only possible via heritage missions with marginal radiometric performances. Landsat-8's improved radiometric performance and the 443-nm band opens opportunities for a wide range of local and national users to better monitor and manage water resources. The recent integration of heritage Landsat data processing into the SeaWiFS Data Analysis System (Pahlevan et al., 2018) allows for long-term studies of aquatic environments using a common processing platform. The science community can further explore long-term consistent water quality products along with Landsat-derived surface temperature products (Laraby and Schott, 2018; Malakar et al., 2018; Schaeffer et al., 2018) to infer the associated intricate relationships in aquatic health status and the ambient water temperature. Current research focuses on developing water-type-specific algorithms and improving the atmospheric correction in CDOM-rich and extremely turbid waters.

Recent analysis of the Landsat archive has advanced our knowledge of surface water dynamics at scales from local to global. By using imagery across multiple years and throughout seasons it has been possible; to map the extent and dynamics of surface water and flooding for entire river basins (Tulbure et al., 2016); to map continental-scale changes in persistent water bodies and ephemeral features (Mueller et al., 2016), lake extents, their distribution plus seasonal and interannual lake area variability (Sheng et al., 2016); to produce global inventories for specific years of lakes (Verpoorter et al., 2014) and all surface water (Feng et al., 2016); to map and separate permanent and seasonal water surfaces at 5 to 10 year intervals globally (Yamazaki et al., 2015); and to show where global surface water occurrence (seasonality and persistence) changed month by month over more than three decades (Pekel et al., 2016). Collectively the above work provides new information to improve hydrology and climate modeling, to identify climate change impacts and threats to biodiversity, to analyze water usage, demand, and stress, to model the spread of waterborne pollution and diseases, to assess desertification, drought and flood risks and occurrences, even for the geopolitics of transboundary water distributions and supplies.

4.1.3. Vegetation phenology

4.1.3.1. Agricultural environments (phenology). Physiological crop growth stages can be related to crop phenological metrics detected using remote sensing data (Sakamoto et al., 2011; Zeng et al., 2016; Gao et al., 2017). Current remote sensing phenology products are normally available from coarse resolution sensors such as MODIS and VIIRS (Zhang et al., 2003). At these scales (≥250-m), crops and fields are frequently mixed, which limits the uses of coarse resolution phenology products over complex and heterogeneous agricultural landscapes. These crop phenological metrics are more useful when mapped at Landsat spatial resolution or at field scale. However, extracting crop phenology at field scale using Landsat imagery is challenging due to the lack of frequent clear Landsat observations.

In recent years, data fusion approaches have been developed to improve temporal sampling at Landsat spatial scales. These spatial and temporal data fusion models allow combining of high frequency yet low spatial resolution imagery (e.g., MODIS and VIIRS) with less frequent but high spatial resolution imagery (e.g. Landsat and Sentinel 2) (Gao et al., 2015). The data fusion approach can bridge large temporal gaps between actual Landsat observations, integrating temporal information from coarser but wider swath imaging sensors. Using the Spatial and Temporal Adaptive Reflectance Fusion Model (STARFM) (Gao et al., 2006), Gao et al. (2017) generated daily surface reflectance and vegetation index at Landsat spatial resolution for central Iowa from 2001 to 2015. Fifteen years of phenological metrics for corn and soybean were extracted at 30-m resolution and compared to crop growth stages from the National Agricultural Statistics Service (NASS) crop progress. Results demonstrated that time series data from multiple sensors effectively detect major crop physiological stages at the field scale. The phenology for corn and soybean crops can be clearly separated and quantified at 30-m resolution. This capability has potential applications in farmland management and crop growth modeling for yield prediction.

Landsat observations can be doubled in areas where two Landsat paths overlap. For example, in the Grape Remote sensing Atmospheric Profile and ET eXperiment (GRAPEX; Kustas et al., 2018) Gallo site near Lodi, California, > 60 clear Landsat-7 and -8 observations each year were obtained from 2013 to 2016. These observations are frequent enough for generating daily vegetation index and grape vine phenology using Landsat data alone (Sun et al., 2017). Combining Landsat and other Landsat-resolution data such as from Sentinel-2 in the process can directly benefit crop phenology mapping. Research is underway to integrate Landsat and Sentinel-2 for extracting crop phenology especially for mapping crop growth stages in real-time, within the growing season.

Crop phenology mapping would benefit from having more frequent Landsat observations and higher spatial resolution (e.g., 10-m). While multi-sensor data fusion has proven effective at simulating Landsat-scale surface reflectances between overpasses, more frequent actual acquisitions are clearly preferable. This is due to several reasons. First, fusion relies on consistency in surface reflectance data between sensors which can be a challenge due to the differences in sensor characteristics, calibration and atmospheric corrections. Second, while fusion works well retrospectively, it is less well adapted for simulating reflectance changes in real time – i.e., beyond the most recent Landsat acquisition. The more frequent the updates, the more accurately crop progress can be tracked. Increasing spatial resolution in the reflectance bands on future Landsat missions to 10-m would enable monitoring of smaller sized fields, which are prevalent in many regions globally (White and Roy, 2015).

4.1.3.2. Forests (phenology). Phenology became central in the Landsat data acquisition strategy with Landsat's Long-Term Acquisition Plan (LTAP) for Landsat ETM+ (Loveland and Dwyer, 2012) that greatly

supports phenology-related studies. In particular, research focusing on forest phenology targets a broad range of scientific questions that are of utmost importance for remote sensing and global change research: First, better understanding forest phenology is core for disentangling the Earth's ecosystems response to ongoing climate change (Broich et al., 2015; Senf et al., 2017a). Second, forest phenology from long-term satellite data allows upscaling forest ecological knowledge from the field to landscape, continental and global scales (Fisher et al., 2006; Melaas et al., 2013; Nijland et al., 2016). Third, better characterizing forest phenology from Landsat allows creating phenological metrics in support of phenology-optimized image compositing, mapping and monitoring (Frantz et al., 2017; Griffiths et al., 2013a; White et al., 2014).

The great variety of global forest phenologies renders mapping and characterization challenging, including issues related to highly diverse seasonality, forest types, or forest densities and height (White et al., 2010). It is therefore not surprising that forest phenology studies have long been the domain of coarse-scale analyses that offer more frequent observations from space. Landsat-based studies on forest phenology therefore often take advantage of various fusion strategies between, for example, Landsat and MODIS (Zhu et al., 2012; Frantz et al., 2017; Baumann et al., 2017).

With recent methodological advances in time series analyses and abundant data being available through Landsat Global Archive Consolidation (LGAC), modeling forest phenology from Landsat data will allow backcasting phenology to the 1980s, which will be core to relate forests phenology to global change (Senf et al., 2017b). As noted in Wulder et al. (2016), the regional yield of imagery available in the Landsat archive varies regionally and temporally, constraining the generality of opportunities especially prior to the combined Landsat-5 and -7 period and the Landsat-8 era. Melaas et al. (2016) have shown that it is feasible to identify the start and end of the growing season in temperate and boreal forests from Landsat time series. While the gradual character of savanna ecosystems in terms of tree height and density poses additional challenges for phenology studies, it seems also possible to separate different savanna subsystems based on their phenological fingerprint (Schwieder et al., 2016). Approaches to produce within-year, gap-filled, series of Landsat data (e.g., Vuolo et al., 2017) offer an example and foreshadow opportunities for improved capture of phenology and phenomena that vary rapidly over space and time. Data blending approaches (across spatial scales) have also been demonstrated to produce bi-weekly, phenologically relevant, outputs (Bhandari et al., 2012).

4.1.4. Albedo, surface temperature

4.1.4.1. Surface albedo. Land surface albedo (the proportion of incoming solar radiation which is reflected back to space from a surface) plays an important role in the Earth's surface energy budget. However, albedo, which is an intrinsic quality of the surface, varies both temporally and spatially as a function of surface type, surface structure/cover, and ecosystem dynamics, with dramatic and rapid alterations occurring in response to seasonal snowfall and melt, water fluctuations and flooding, and vegetation phenology, as well as to disturbance and recovery processes.

Moderate resolution cloud-free, near-nadir imagery from the Landsat series provides information on surface heterogeneity, vegetation status, and biomass extent, but cannot provide adequate multi-angle observations to accurately capture the true effects of surface anisotropy (i.e., bidirectional reflectance distribution function, BRDF) and produce realistic bi-hemispherical albedo quantities of the surface. However this angular information can be derived from coarser resolution, wide swath, multi-angle imagers such as MODIS and VIIRS (Lucht et al., 2000; Schaaf et al., 2002; Wang et al., 2014; Campagnolo et al., 2016). Thus, Landsat-8 land surface albedo is derived by coupling Landsat observations with MODIS or VIIRS BRDF information (Shuai et al., 2011). This provides true Landsat albedo at more appropriate spatial resolution needed for a number of land surface applications, including monitoring of forests, agricultural fields, impervious surfaces in urban areas, areas affected by insect, wildfire or storm damage, and other heterogeneous and dynamic environments such as shorelines and wetlands (Mihailovic et al., 2004; Barnes and Roy, 2010; Wang et al., 2016; Andrews et al., 2017). Furthermore, albedo can vary significantly over snow and snow-free surfaces with significant climate implications (Betts, 2000) that may be more appropriately resolved at Landsat resolution. Thus far, Landsat-8 snow and snow-free albedo have good agreement with field measured albedo (RMSEs of < 0.05) from a range of spatially representative sites of the International Baseline Surface Radiation Network (BSRN), NOAA's Surface Radiation Budget Network (SURFRAD), the Arctic Observatory Network (AON), and the Ameriflux network (Wang et al., 2016).

4.1.4.2. Surface temperature. A Landsat-8 surface temperature product has been developed (Malakar et al., 2018). Initially it was expected that this product would take advantage of the two thermal bands available on the Landsat-8 TIRS instrument. Given stray light/ghosting issues (Montanaro et al., 2014) the product is based on a single-band solution, and hence applicable to the entire Landsat thermal archive and uses Landsat-8 band 10 (10.60–11.19 μm) due to its better calibration. The Landsat surface temperature product has undergone testing on Landsat-5 and -7 data using water surface temperatures as truth. The product uses global reanalysis data and elevation in conjunction with the MODerate resolution atmospheric TRANsmission (MODTRAN) radiative transfer code to estimate atmospheric transmission path radiance and downwelling radiance on a per pixel basis (Cook et al., 2014). It uses ASTER derived emissivity data modified by Landsat derived NDVI values to estimate per-pixel emissivity (Hulley and Hook, 2009).

Surface temperatures derived from the NOAA moored buoy fleet have been compared to Landsat-5 derived surface temperatures using North American Regional Reanalysis (NARR) data (Mesinger et al., 2006). The results were encouraging for the 25 cloud-free sites available (no clouds within 5–10 km of the buoy) showing residual errors in the derived temperature of $-0.2\,\mathrm{K} \pm 0.89\,\mathrm{K}$. These results also showed increasing error with clouds in the surrounding area which prompted a more global study. The resulting global study used MERRA reanalysis data (Rienecker et al., 2011) as input to the atmospheric parameter retrievals and “best quality” MODIS derived sea surface temperature data for truth. This was required because the buoy and NARR data were only available for North America. The data covered a wide range of atmospheric conditions across the globe. In all, 3196 sites were studied using cloud-free Landsat-7 ETM+ data and provided a mean error of 0.2 K and an RMSE of 1.77 K. The errors increased when the site was close to clouds or the atmospheric transmission was low. For the 1395 sites with cloud distances > 5 km and transmission values > 0.55 the expected RMSEs were reduced to 1.02 K (Laraby and Schott, 2018).

4.1.5. Water use and crop yield (evapotranspiration)

Evapotranspiration (ET), the flux of water vapor from the land surface to the atmosphere, is the second largest water budget component after precipitation. Quantifying ET is fundamental for understanding energy and water budgets at global to field scales, and the ability to produce a detailed accounting of water use will promote more sustainable management of our freshwater resources. Over the past decade, the use of Landsat optical and thermal data for water and agricultural management has greatly increased (Anderson et al., 2012; Leslie et al., 2017). This is due, in part, to the Landsat open-data policy as of 2008, coupled with advances in automation of ET algorithms and high-performance computing. These developments have catapulted Landsat-based ET research and applications to the forefront of water management, particularly in the western U.S. (Willardson, 2014).

Landsat's spatial resolution and coincident reflectance and thermal

band(s) provide the means to accurately and consistently quantify water consumption over large areas and long time periods, and at field scale - the scale at which water and agriculture is managed. Surface temperature forms the basis for ET estimation by many commonly used Landsat-based surface energy balance algorithms by exploiting the fact that ET consumes energy and therefore cools the land surface (Anderson et al., 2011; Kalma et al., 2008; Allen et al., 2007). Reflectance based algorithms that rely on vegetation indices such as NDVI have shown utility for estimating ET from irrigated crops that have ample water supply with dry or little exposed wet soil (e.g., Melton et al., 2012), as well as during the cool season where the surface temperature contrast between wet and dry fields is reduced. Vegetation Index approaches are less well-suited for routine satellite monitoring of actual water use over rainfed agricultural lands and natural systems such as wetlands (Fig. 5), or for detecting onset of stressed conditions (Anderson et al., 2012). Thermal band imagery at field scale can effectively capture the elevated soil and canopy temperature signals that accompany moisture deficiency and stress, serving as a high-resolution proxy for surface soil moisture measurements.

ET information at scales discriminating different crop types can be used for water accounting (Karimi et al., 2013) and for scheduling irrigation applications (Kustas et al., 2018). Globally, demand for field-scale ET information for food and water security applications is ever increasing (Fisher et al., 2017). In combination with time series of surface reflectance data, Landsat ET time series can be used to assess changes in water use that accompany changes in land cover and land use (Anderson et al., 2018). As a result, state-level compliance management and monitoring authorities now use Landsat-based ET maps to complement pumpage inventories, estimate groundwater recharge and discharge, and for assessing interbasin transfers of groundwater (Beamer et al., 2013; Huntington et al., 2016).

Thermal-based ET retrievals are also being used to advance the detection of agricultural drought and resulting impacts on crop yields. The Evaporative Stress Index (ESI), quantifying standardized anomalies in the actual-to-reference ET ratio at regional scale using thermal imagery from geostationary satellites, has demonstrated capability for early detection of rapid onset ("flash") drought impacts and associated crop stress, both within the U.S. and internationally (Anderson et al., 2013, 2016a, 2016b; Otkin et al., 2016). However, the 3–5 km pixel resolution afforded by geostationary, and moderate resolution thermal sensors like MODIS, cannot resolve crop stress signatures in individual farm fields, providing a blended signal from multiple crop types and management strategies. Yang et al. (2018) demonstrated that when disaggregated to 30-m resolution using Landsat TIR and reflectance band imagery, ESI has the capacity to capture developing stress signals and predict resulting yield reductions. Field-scale ESI is being integrated with Landsat-Sentinel-MODIS fused vegetation index time series (Gao et al., 2018) and phenology products (see Vegetation phenology sub-section) within a regional yield-modeling framework to account for impacts of moisture stress occurring during phenologically sensitive stages of crop growth.

4.1.6. Forest monitoring

Changes in forest ecosystems result in a variety of ecosystem responses (Vogelmann et al., 2012) that are influenced by many factors and vary according to the magnitude and nature of the change. Repeat measurements of forest ecosystems through time enable the characterization of an ecosystem's response to change (via the temporal trajectory of observations), and the more measurements that are acquired, the greater the likelihood that both the change—and the ecosystem's response to that change—will be accurately captured (Kennedy et al., 2014). Free and open access to the temporally extensive Landsat archive in 2008 fundamentally changed the manner in which Landsat data are used for forest monitoring (Banskota et al., 2014). In a forest monitoring context, Landsat time series has allowed for movement beyond a focus on binary identification of whether or not a stand-replacing change has occurred, enabling the characterization of a much broader range of change types, magnitudes, and directions as well as pre- and post-change conditions.

Numerous disturbance mapping algorithms and approaches using Landsat time series data have emerged (see review by Zhu, 2017), with each algorithm having a range of capabilities for detecting both gradual and discrete disturbance events (Cohen et al., 2017). These algorithms, using either cloud-free image composites (Griffiths et al., 2013a; White et al., 2014) or every clear image pixel (Zhu and Woodcock, 2014a; Brooks et al., 2014), and unconstrained by computational limitations (Hansen et al., 2013), have enabled the accounting of forest dynamics over long time frames and large areas, using both sample-based (Masek et al., 2013) and spatially extensive mapping approaches (Griffiths et al., 2014; Hansen et al., 2013; Potapov et al., 2015; White et al., 2017). While the capacity for comprehensive forest monitoring over large areas has been demonstrated, Landsat time series data have also enabled other methodological improvements in forest monitoring, such as the development of approaches for automating the attribution of disturbance type (e.g. fire, harvest, windthrow) (Schroeder et al., 2011; Hermosilla et al., 2015b; Schroeder et al., 2017; Oeser et al., 2017),

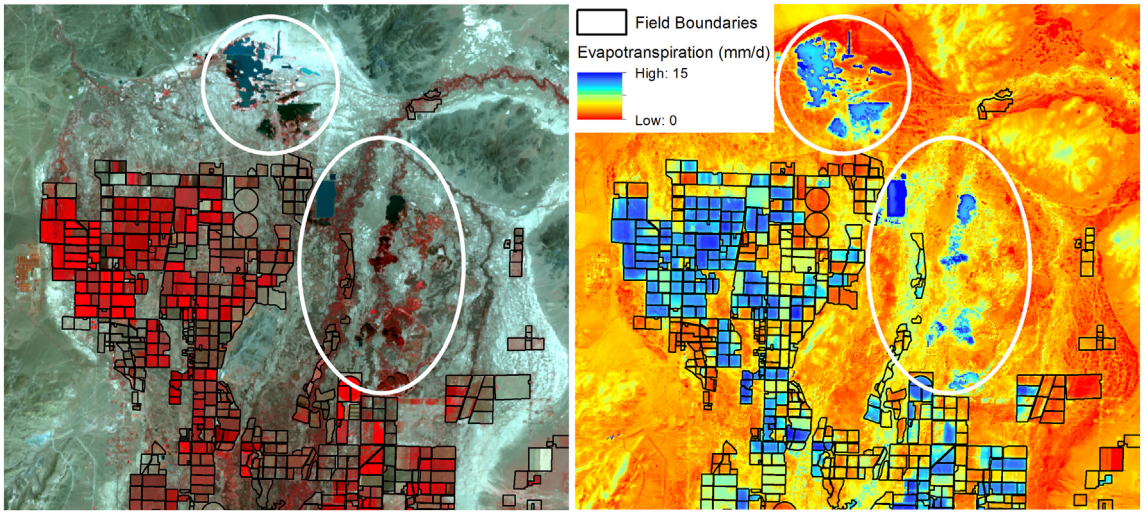

Fig. 5. Landsat-8 false color infrared (left) and TIRS-based retrieval of ET (following Allen et al., 2007) (right) over Mason Valley, NV from July 29, 2015. Landsat's TIRS detects evaporation from soil, wetlands, and open water areas, whereas common vegetation index bands such as near-infrared do not as shown by areas of low reflectance with relatively high evaporation (e.g. areas within white ellipses).

characterizing post-disturbance regrowth and recovery (DeVries et al., 2015; Frazier et al., 2015; Chu et al., 2016; Pickell et al., 2015; Frazier et al., 2018; White et al., 2018) and differentiating recovery trends by disturbance type (Madoui et al., 2015; White et al., 2017), as well as characterizing the temporal dynamics of forest fragmentation (Hermosilla et al., 2019). Landsat time series have also provided new opportunities to detect and evaluate more gradual and non-stand-replacing disturbances related to pests, disease, and drought (Goodwin et al., 2008; Meigs et al., 2011; Vogelmann et al., 2012; Senf et al., 2015; Pasquarella et al., 2017; Ahmed et al., 2017).

Methods and approaches for using Landsat time series to understanding of post-disturbance recovery, forest decline, and the impacts of climate change in forests will likely continue to be a focus of ongoing and future research (McDowell et al., 2015; Cohen et al., 2016). Likewise, the development of methods that enable the full integration of MSS data into forest monitoring approaches will further extend the baseline of disturbance history (Vogeler et al., 2018). While the majority of studies noted above have focussed on the use of 30-m Landsat data from TM, ETM+, and OLI sensors, Pflugmacher et al. (2012) demonstrated the utility of incorporating the full Landsat record (e.g., 1972 forward), inclusive of MSS data, for characterizing forest dynamics.

5. Outlook

5.1. Importance of Landsat to international science and monitoring programs

Since Landsat-1 acquired its first image in 1972, the global human population has almost doubled (UNDESA, 2017), atmospheric CO_2 concentration has increased by around 25% (Keeling and Whorf, 2005), 10 to 20% of the world's drylands are affected by land degradation (Reynolds et al., 2007), total forest area has shrunk by around 3% (Keenan et al., 2015), and biological diversity has been in almost continuous decline (Butchart et al., 2010). Such trends have not gone unnoticed by the world's policymakers: the 1992 UN Conference on Environment and Development, held in Rio de Janeiro, put in place provisions leading to the UN Framework Convention on Climate Change (UNFCCC), the Convention on Biological Diversity (CBD) and the UN Convention to Combat Desertification (UNCCD). International consensus-building on environmental issues has, in fact, continued throughout the Landsat Program's lifetime, perhaps reaching an apogee in the 2030 Agenda for Sustainable Development, with its 17 Sustainable Development Goals (SDG) and 169 targets (UN, 2015).

The Rio Conventions recognize the importance of systematic observations, and all three have identified priorities; Essential Climate Variables for the UNFCCC (Dolman et al., 2016; GCOS, 2016), Essential Biodiversity Variables for CBD (Pereira et al., 2013; Pettorelli et al., 2016) and Progress Indicators for the UNCCD (Sommer et al., 2011; UNCCD, 2013). Progress towards the SDG targets is also being measured through indicators, currently well over 200 of them (UNESC, 2017). The variables and indicators requested by these Multilateral Environmental Agreements (MEAs) vary in terms of the detail with which they are defined; some are expressed by metrics including frequency (days, years, decades) and geospatial resolution (m, km, country/region), others are more qualitative. Variables and indicators where Landsat has made a significant contribution, and where further research is a priority, are presented in UNFCCC (GCOS, 2016), CBD (Pettorelli et al., 2016), UNCCD (UNCCD, 2013), SDG (UNESC, 2017) (i.e., satellite-derived glacier area, lake area, burned area, land cover and land use change).

One example of the above is the UNFCCC's mechanism to 'reduce emissions from deforestation and forest degradation, and the role of conservation, sustainable management of forests and enhancement of forest carbon stocks' (REDD+). This mechanism came into existence partly *because* it could be monitored (De Sy et al., 2012), and this monitoring was possible *because* of the Landsat program's spatial and temporal coverage; the steps involved in REDD+ accounting specify the use of 'Landsat-type remotely sensed data' for monitoring changes in forest area, and note that the Landsat archive is currently the 'only free global mid-resolution (30 m) remote sensing imagery' covering the necessary years (GOFC-GOLD, 2016).

5.2. The role of Landsat as a reference instrument

Since 2000 the world of civilian satellite remote sensing has changed dramatically (Belward and Skøien, 2015). No longer are there only a small number of instruments in space that provide imagery for science and commercial purposes. Today, there are dozens of commercial companies and many nations that are developing their own systems (Butler, 2014) with a capacity to address increasingly complex questions and information needs (Finer et al., 2018). For example, the number of satellites in the PLANET constellation has been increased to provide near daily global coverage 3-m multi-spectral data (Strauss, 2017). Thus, the question that surfaces becomes, 'What is the role of a science grade moderate resolution government satellite in a commercial world of hundreds of imaging satellites?" This becomes especially critical when comparisons are made of the resources necessary to launch and operate a Landsat-class sensor as opposed to a 'smallsat' sensor. A key role that is essential for the optical satellite remote sensing community, and one that can only be fulfilled by a science-grade legacy instrument system, is that of providing an anchor, or reference point, by which other systems can be compared (Schingler Jr., 2015). It is critical, not only for the scientific community but also for the commercial community, to be able to use data from multiple sources and combine them in a consistent manner that allows extraction of information that would otherwise be unavailable. If this cannot be achieved, then the usefulness of these systems is compromised. It is useful to note that the use of commercial high spatial resolution data sources comes with a number of costs, including financial (to purchase), computing (to process and store), and management (to organize and access) (Wulder et al., 2008). Depending on the geometric and radiometric quality of a given high resolution data source, automated approaches may be precluded, with costly user interventions required.

Landsat sits in a unique position to fulfill this role. For many years it has been referred to as a 'gold standard' by which other sensors have been compared (Goward et al., 2017). This is due to its historical legacy, availability of data, global imaging, and to its superior calibration. Thus, it serves as the central reference point to which most moderate and high resolution optical satellite systems are compared to today. Landsat-8, in particular, boasts a stable radiometric performance since its launch providing traceable, consistent TOA reflectance observations across a wide dynamic range, i.e., over land, snow/ice, and water bodies (Helder et al., 2018). In order to fulfill this vital role, Landsat must continue to be a reference radiometer against which all other satellite payloads have their performance gauged against. This implies that it must continue to excel in the production of the highest quality data. In order to do so, radiometric, geometric, and spatial calibration must continue to be improved so that the uncertainties associated with TOA and surface products can be reduced. Furthermore, labeling each TOA observation (pixel) and the derived surface reflectance products with associated uncertainties enables a rigorous and traceable intercomparison analysis.

5.2.1. Thermal infrared, TIRS

The long archive of global, moderate resolution thermal imagery collected by the Landsat series since 1982 is unmatched by any other satellite program, and will continue to be an invaluable asset to better manage Earth's water resources. In the early planning for the Landsat Data Continuity Mission, the thermal component was omitted as a cost-savings measure. The ultimate inclusion of TIRS on Landsat-8 was the culmination of successful demonstration of the science and application

imperatives to maintain continuity of the archive and legacy of Landsat thermal imagery and to support operational water management applications (Willardson, 2014).

The TIRS imager brought new quantum well (QWIPS) technology to Landsat, providing a pushbroom system with 100-m spatial resolution and a substantial increase in SNR over previous Landsat systems (Reuter et al., 2015). Using Landsat-8 TIRS, the thermal community has created and expanded new applications fronts that use the concurrently collected thermal and reflected Landsat data of Landsat-8 and previous Landsats to retrieve ET, surface energy components, and water use information (Burkhalter et al., 2013; Hendrickx et al., 2016; de la Fuente-Sáiz et al., 2017; Anderson et al., 2018). Besides utility for ET mapping, Landsat thermal imagery have been demonstrated to substantially improve cloud and shadow detection and mapping (Zhu and Woodcock, 2012; Zhu et al., 2015b). The higher SNR of TIRS on Landsat-8 and new means for calibration has provided new capacity to monitor water quality (Cook et al., 2014) and as input to specifications for future TIRS imagers (Cui et al., 2015). NASA and Landsat Science Team efforts have mitigated the ghosting problem with the TIRS imager that were largely compensated for by correction using contextual radiance from the ghosting source (Montanaro et al., 2015). The cause of ghosting has been identified and will be corrected for Landsat-9 (Montanaro et al., 2014).

In preparation for future Landsat missions, the importance of more frequent thermal-imaging to mitigate the effects of clouds on monthly and annual ET retrievals at the field scale has been demonstrated. Anderson et al. (2012) have shown that a single Landsat satellite having 16-day return time satisfied temporal requirements for time-varying ET only two years (8%) out of the 26-year Landsat archive for a relatively 'clear' region of southern Idaho. With a second satellite having the same 16-day return time, but with an 8-day offset from the first satellite, the number of years successfully meeting time-based requirements for ET increased to four years out of ten (40%). With a 4-day return, the requirement of one monthly clear-sky image was met in 70 to 80% of all years. More humid regions of the US, such as the Midwest, have relatively cloudy images that require an even shorter image revisit interval for high levels of success. A minimum four-day return time for thermal imaging is recommended for successful ET retrievals over large portions of the globe. Quantifying the value of increased temporal sampling in high resolution TIR imaging is one objective of the ECOsystem Spaceborne Thermal Radiometer Experiment on Space Station (*ECOSTRESS*) research mission, launched in June 2018. The unique orbital pattern of the International Space Station will allow frequent multi-band thermal imaging at Landsat-like spatial resolution (~70-m) and a nominal 4-day interval, but as frequently as several images per day. The increased accuracy in surface temperature retrievals afforded by multiple thermal bands and the ability to additionally retrieve surface emissivity (Hulley et al., 2012) make this a promising configuration for future Landsat missions.

5.2.2. MSS

MSS data were acquired systematically by Landsat-1 to -3 from 1972 to 1983 and intermittently by Landsat-4 and -5 from 1982 to 2012 (Goward et al., 2006). As of early 2016 there were over 1.2 million MSS images in the US archive, with close to two million expected after completion of the global archive consolidation project (Wulder et al., 2016). At the time of writing there are no MSS ARD products (Dwyer et al., 2018). ARD MSS processing is challenging because the MSS had no shortwave infrared or thermal wavelength bands and coarser spatial, spectral and radiometric resolution compared to the later Landsat sensors. Using MSS data in time series analyses has become more easy, given the new Landsat Collection strategy. However, because of its native 57-m × 79-m spatial resolution, most MSS data cannot meet the image-to-image georeferencing tolerance of ≦12-m radial RMSE for Tier 1 of the Collections and are placed in Tier 2. In addition, MSS data were collected with 6-bit radiometric resolution and the four spectral bands (red, green and two near-infrared) do not match those of the later Landsat sensors. As a result, reliable MSS atmospheric correction and cloud masking is difficult to implement. These serious trade-offs, however, are dwarfed when the science or application information need requires Landsat data collected before 1985. For these years MSS is a unique data record; for 13 years (1972–1984) MSS are the only source of global data for applications requiring moderate resolution digital satellite data.

Conceptually, there are two primary pathways for using MSS data for time series analyses through the full archive: temporal splicing, and temporal harmonization. Temporal splicing would analyze the MSS data independent of the TM/ETM+/OLI portion of the archive. This could involve time series algorithms described in Cohen et al. (2017) and elsewhere. Because there is overlap in coverage by both MSS and TM between 1982 and 1995, there would be two sets of predictions for that period. Ideally, the mapped change results for the overlapping period would be the same for both datasets, and a simple concatenation would suffice after trimming the last several years of MSS results (1982–1995). More likely, however, there will be cases with some mapped differences in the overlapping period; e.g., for a given pixel, a subtle disturbance identified between 1987 and 1988 represented by a minor spectral change followed by a two-year spectral recovery in the MSS series and no disturbance (and hence no recovery) mapped for that period in the TM series. In circumstances such as these, a logic would be required to blend or splice the two sets of results at the pixel-level. Splicing would be complicated by consideration of the spatial resolution difference between the two sensors.

Temporal harmonization would involve derivation of adjustment equations to translate MSS spectral bands into TM spectral bands or vegetation indices using statistical regression approaches applied to near contemporaneous data (e.g., Roy et al., 2016a) or to coincident under flight data (e.g., Holden and Woodcock, 2016). However, because MSS data have reduced resolution and different spectral band passes compared to TM data more research is required. Despite these issues, a process for harmonizing MSS and TM data has been developed which includes cloud and cloud shadow masking a (Braaten et al., 2015) and provides MSS TOA reflectance adjusted to the equivalent TM bands (Fig. 6).

5.2.3. Landsat/Sentinel-2

The launch of the Sentinel-2 constellation, part of the European Union's Copernicus Earth Observation program, has dramatically changed the landscape for land observations. As the "Landsat-like" component of Copernicus, Sentinel-2 shares many of the technical characteristics of the existing Landsat system. While Sentinel-2 does not have a thermal infrared capability, the wider (290 km) swath and two-platform constellation, Sentinel-2A (launched 2015) and Sentinel-2B (launched 2017), provides routine 5-day revisit over Earth's land areas at a spatial resolution of 10 to 60 m (Drusch et al., 2012). In addition, Sentinel-2 provides unique features not available from Landsat, including red-edge and water vapor spectral bands, as well 10-m and 20-m visible to shortwave infrared bands that are higher spatial resolution than the Landsat-8 30-m bands.

Landsat-8, Sentinel-2A, and Sentinel-2B together provide a global median average revisit interval of 2.9 days (Li and Roy, 2017). This opens up the possibility of mapping processes that are highly dynamic in time, including vegetation phenology, fire dynamics, and coastal/inland water quality. In principle, this combination of temporal frequency and spatial resolution provides a "30-m MODIS" virtual observatory, with the ability to extract highly dynamic biophysical processes at sub-hectare resolution (Wulder et al., 2015). With the launch of Landsat-9 planned for late 2020, this virtual constellation will become even more frequent approaching a 2-day revisit cycle.

Recognizing this opportunity, researchers have been actively engaged in finding ways to use Sentinel-2 and Landsat together. The NASA Multi-source Land Imaging (MuSLI) program has supported

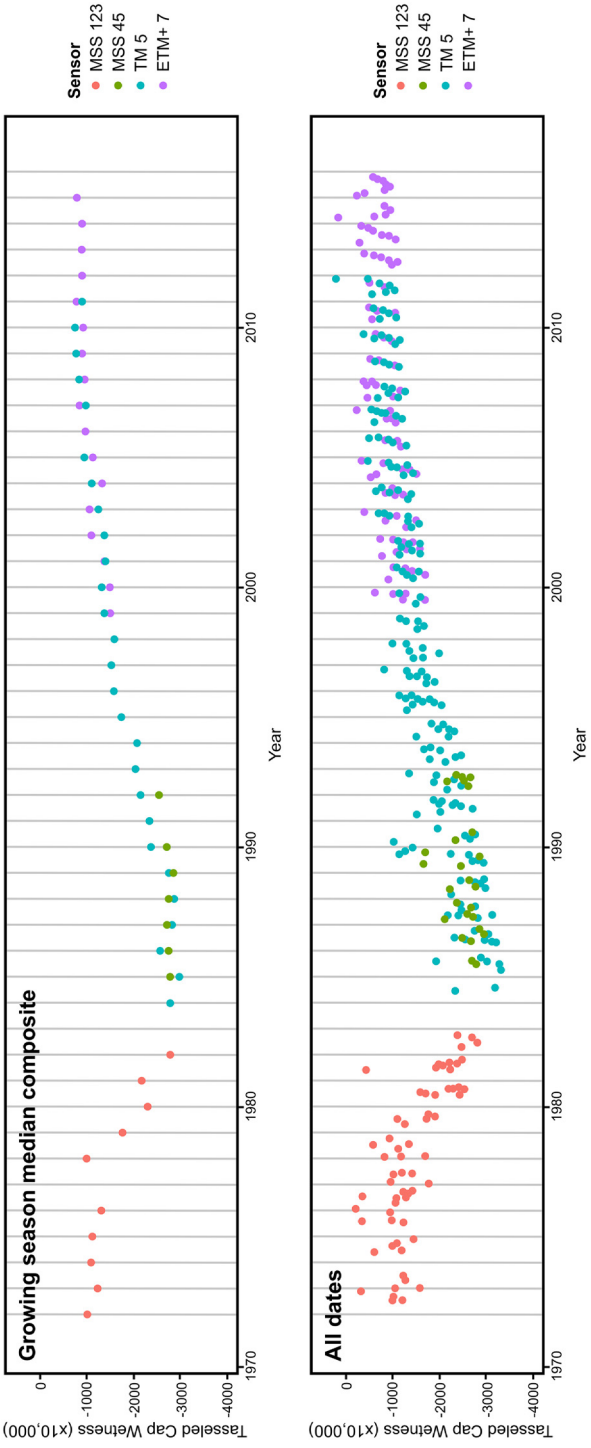

Fig. 6. Example of single Landsat pixel including MSS, TM, and ETM + (Upper panel: median composite of peak growing season observations; Lower panel: all clear observations). Note there is a gradual change from 1972 to 1982 and followed with a post-disturbance recovery from 1987 to 2010.

prototyping activities for new land science products, including burned area mapping, forest phenology studies, and improved mapping fractional water characterization (Torbick et al., 2018). Similar work is underway in Europe through Copernicus services and national monitoring activities. The Harmonized Landsat/Sentinel-2 (HLS) project at NASA GSFC has focused on the necessary radiometric and geometric corrections to generate a seamless surface reflectance product using both sensors as inputs (Claverie et al., 2018). These activities have been complemented by members of the NASA/USGS Landsat Calibration Team and the ESA Sentinel-2 Validation Team, who have collaborated to demonstrate that the measurements from Landsat-8 OLI and Sentinel-2 Multi-Spectral Imager (MSI) agree to within their individual uncertainties (Pahlevan et al., 2018; Barsi et al., 2018).

Despite the evident promise, however, a variety of technical challenges remain. Pixel-level co-registration between Landsat and Sentinel-2 has been problematic (Storey et al., 2016), an issue that should be ameliorated by the use of shared ground control beginning in 2019 and reprocessing of the Landsat archive to Collection 2. In the interim, approaches to register the data have been developed (Yan et al., 2016; Skakun et al., 2017). Atmospheric correction, cloud and shadow masking algorithms are being developed for both sensors (Doxani et al., 2018) but currently without a consensus approach. The differing swath width and orbit tracks result in sun- and view-angle variability between the sensors for any given ground target and cause reflectance variations that will be non-negligible for certain applications (Roy et al., 2016b, 2017). Methodologies to statistically calibrate reflectance differences between Landsat-8 and Sentinel-2 imposed in particular by sensor spectral band response differences are being developed (Claverie et al., 2018; Zhang et al., 2018). In addition, the processing system baselines and Level-2 (surface reflectance) approach for both data sets, in particular the more recent Sentinel-2 data (Gascon et al., 2017), have changed quite frequently. New algorithms are being developed within the remote sensing community to mitigate these issues and create "harmonized" products from the combined sensor stream, but there remains room for improved coordination between US agencies and ESA.

5.3. Landsat-9

In 2015, NASA directed Goddard Space Flight Center (GSFC) to begin implementing the Landsat-9 mission as the first step in the interagency Sustainable Land Imaging (SLI) Program, which seeks to maintain continuity of moderate-resolution observations through the 2030s. Given that the end of life for Landsat-7 is projected for summer of 2021 due to fuel supply, coupled with the need to maintain 8-day revisit continuity, NASA moved forward with Landsat-9 as a near-rebuild of Landsat-8. Landsat-9 will carry two instruments, the Operational Land Imager-2 (OLI-2) built by Ball Aerospace Technologies Corp. and the Thermal Infrared Sensor-2 (TIRS-2) built by GSFC. Northrup Grumman Innovation Systems of Mesa, Arizona, is building the spacecraft, and General Dynamics (under contract to USGS) will build the Mission Operations element. Launch of Landsat-9 is scheduled for December 2020. While Landsat-9 OLI-2 is virtually identical to Landsat-8 OLI for measuring solar-reflected wavelengths, Landsat-9 TIRS-2 features some upgrades. The original Landsat-8 TIRS had an optical design problem that caused stray radiance from outside the field of view to enter the focal plane, degrading the radiometric accuracy of the instrument (Montanaro et al., 2014). Also, the encoder for the TIRS scene select mirror stopped operating early in the mission. These problems have been addressed in the revised TIRS-2 design. Because TIRS was a late addition to the Landsat-8 mission payload, its design had little redundancy with only a 3-year design (risk class "C") life. Landsat-9 TIRS is being designed to meet 5-year (risk class "B") requirements.

The Landsat ground system at USGS EROS has undergone improvements with development of a multi-mission operations center that will support both Landsat-8 and -9 operations and will increase the

computational efficiency of data processing, archiving, management and distribution. Landsat-9's daily imaging capacity will be on par with Landsat-8 at ~740 scenes per day even though the mission requirement remains at 450. Landsat-9's long-term acquisition plan (LTAP) will mimic Landsat-8 and continue with global land imaging of all sunlit landmasses and near shore coastal regions at a solar elevation greater than 5°. The anticipated science value and enhancements of Landsat-9 will be anchored by sustained 8-day global land imaging to support numerous operational application dependencies, utilization of all 14 bits to further resolve pixel to pixel radiometric resolution, and a higher degree of absolute radiometric calibration accuracy that will certainly improve the radiometric calibration for Landsats 1–8.

5.4. Landsat-10

The charge for Landsat-10 under guidance from the SLI program is to advance measurement capability while preserving continuity and constraining program costs. Currently, all options are being considered for Landsat-10 including new, compact imaging technologies, international partnerships, and involvement of the commercial sector. While the system may not be simply an improved Landsat-9, or a single satellite, continuity with historic measures data record will be maintained. NASA is currently investing in technology and technology demonstrations to support the SLI program. These investments span instrument components to full end-to-end instrument concepts that include multispectral and imaging spectrometer designs. Since 2016, the USGS has been gathering input on science requirements and needs from the Landsat user community among other key stakeholders to inform the next generation of Landsat instruments and data. Science and measurement requirements are used to guide system architecture.

Other considerations for the Landsat-10 architecture will include identifying measurement synergies with other international satellite systems such as Copernicus/ESA Sentinel-2 series under the framework of multi-source land imaging that seeks to fuse measurements from a variety of remote sensing technologies to improve temporal revisit frequency for example. Further, the commercial space industry has been rapidly growing and now offers a range of cube and/or small satellite concepts that are currently under evaluation where data products are being compared against Landsat-8 as the current reference standard.

The USGS-NASA Landsat Science Teams have been active over the past several years in contributing to the definition of Landsat-10's science requirements and data product specifications. Through this process, the Landsat Science Team has used temporal frequency, spatial resolution, spectral coverage and resolution, and radiometric resolution as guiding principles during the scoping process. Key conclusions revolve around increasing the temporal revisit to 3–5 days cloud-free, increasing the spatial resolution for most bands from 30 to 10 m, adding targeted spectral bands that improve atmospheric characterization and enhance or broaden emerging Landsat science applications, and maintain if not exceed Landsat-8 OLI's on-orbit radiometric performance.

6. Conclusions

Science and resource management communities have benefited from Landsat mission continuity, open access to new and historic imagery, mature and developing ground systems, and an increasingly broad suite of image data products. Free and open access to Landsat imagery has fostered the use of Landsat data to address innumerable science questions, improve resource management, inform reporting activities, and to support an increasingly large user base that is undertaking sophisticated, integrated, and often unprecedented analyses. Over the last decade, the Landsat program has looked both forward and backward. The launch of Landsat-8 secured short-term continuity of Landsat observations, and the planned 2020 launch of Landsat-9 provides further continuity of measures and an ability to plan science and operational capabilities assuming an ongoing data stream. The LGAC initiative gathered and made available via the USGS otherwise inaccessible data. Notably, LGAC resulted in a more than doubling of the number of images in the USGS Landsat archive; an effort equivalent to the launch of an additional Landsat sensor.

Ground systems are a critical element of the Landsat program, ensuring a means to get data from the satellite to the users. The USGS has demonstrated a strong commitment to investing in ground systems, providing imagery in increasingly seamless and analysis ready forms. The policy decision to make Landsat data free and open access has demonstrated the innovations possible when users can access all available data. As a result, recent Landsat science and applications are well represented by time series. Users have availed upon the open access archive to uncover novel insights on the changes to the earth system, with linkages made to human activities. Multiple years of data allow for determination of trends beyond the focused capture of bitemporal change. Indeed, the longevity and resulting temporal dimension of Landsat has emerged as one of the program's greatest innovations.

The Landsat Science Team working in partnership with the leading government agencies (USGS and NASA) enables the provision of science-based, objective inputs on the Landsat program. The Landsat Science Team has played – and is poised to continue to play – this important role in representing Landsat program user needs. The spectral measurements made by Landsat are calibrated and allow for Landsat to operate as a reference instrument, adding value to commercial satellite data and applications. The Landsat Science Team also articulated the science motivation for bringing MSS data in line with that of TM and subsequent Landsat instruments and offering options to produce reliable, continuous measures across all Landsat sensors. Looking forward, the Landsat Science Team will offer insights on virtual constellations of satellites (e.g., Landsat and Sentinel-2), use of Landsat-9, and specifications for Landsat-10.

Acknowledgements

The United States Geological Survey (USGS) and the National Aeronautics and Space Administration (NASA) are gratefully acknowledged for support and encouragement of the 2012–2017 Landsat Science Team (https://landsat.usgs.gov/landsat-science-teams). The Editor and Reviewers are thanked for the valuable insights and constructive suggestions made to improve this manuscript.

References

Ahmed, O.S., Wulder, M.A., White, J.C., Hermosilla, T., Coops, N.C., Franklin, S.E., 2017. Classification of annual non-stand replacing boreal forest change in Canada using Landsat time series: a case study in northern Ontario. Remote Sens. Lett. 8 (1), 29–37.

Allen, R.G., Tasumi, M., Trezza, R., 2007. Satellite-based energy balance for mapping evapotranspiration with internalized calibration (METRIC)—model. J. Irrig. Drain. Eng. 133 (4), 380–394.

Alley, K.E., Scambos, T.A., Anderson, R.S., Rajaram, H., Pope, A., Haran, T.M., 2018. Continent-wide estimates of Antarctic strain rates from Landsat 8-derived velocity grids. J. Glaciol. 64 (244), 321–332.

Alonzo, M., Van Den Hoek, J., Ahmed, N., 2016. Capturing coupled riparian and coastal disturbance from industrial mining using cloud-resilient satellite time series analysis. Sci. Rep. 6.

Anderson, M.C., Kustas, W.P., Norman, J.M., Hain, C.R., Mecikalski, J.R., Schultz, L., González-Dugo, M.P., Cammalleri, C., d'Urso, G., Pimstein, A., Gao, F., 2011. Mapping daily evapotranspiration at field to continental scales using geostationary and polar orbiting satellite imagery. Hydrol. Earth Syst. Sci. 15 (1), 223–239.

Anderson, M.C., Allen, R.G., Morse, A., Kustas, W.P., 2012. Use of Landsat thermal imagery in monitoring evapotranspiration and managing water resources. Remote Sens. Environ. 122, 50–65.

Anderson, M.C., Hain, C.R., Otkin, J.A., Zhan, X., Mo, K.C., Svoboda, M., Wardlow, B., Pimstein, A., 2013. An intercomparison of drought indicators based on thermal remote sensing and NLDAS-2 simulations with U.S. drought monitor classifications. J. Hydrometeorol. 14, 1035–1056.

Anderson, M.C., Zolin, C., Sentelhas, P.C., Hain, C.R., Semmens, K.A., Yilmaz, M.T., Gao, F., Otkin, J.A., Tetrault, R., 2016a. The evaporative stress index as an indicator of agricultural drought in Brazil: an assessment based on crop yield impacts. Remote Sens. Environ. 174, 82–99.

Anderson, M.C., Hain, C.R., Jurecka, F., Trnka, M., Hlavinka, P., Dulaney, W., Otkin, J.A., Johnson, D., Gao, F., 2016b. Relationships between the evaporative stress index and winter wheat and spring barley yield anomalies in the Czech Republic. Clim. Res. 70, 215–230.
Anderson, M.C., Gao, F., Knipper, K., Hain, C., Dulaney, W., Baldocchi, D.D., Eichelmann, E., Hemes, K.S., Yang, Y., Medellín-Azuara, J., Kustas, W.P., 2018. Field-scale assessment of land and water use change over the California Delta using remote sensing. Remote Sens. 10, 889.
Andrews, T., Betts, R.A., Booth, B.B.B., Jones, C.D., Jones, G.S., 2017. Effective radiative forcing from historical land use change. Clim. Dyn. 48 (11), 3489–3505.
Banskota, A., Kayastha, N., Falkowski, M., Wulder, M.A., Froese, R.E., White, J.C., 2014. Forest monitoring using Landsat time-series data—a review. Can. J. Remote. Sens. 40, 362–384.
Barnes, C.A., Roy, D.P., 2010. Radiative forcing over the conterminous United States due to contemporary land cover land use change and sensitivity to snow and interannual albedo variability. J. Geophys. Res. 115 (G4), G04033.
Barsi, J.A., Lee, K., Kvaran, G., Markham, B.L., Pedelty, J.A., 2014a. The spectral response of the Landsat-8 operational land imager. Remote Sens. 6 (10), 10232–10251.
Barsi, J.A., Schott, J.R., Hook, S.J., Raqueno, N.G., Markham, B.L., Radocinski, R.G., 2014b. Landsat-8 thermal infrared sensor (TIRS) vicarious radiometric calibration. Remote Sens. 6 (11), 11607–11626.
Barsi, J.A., Alhammoud, B., Czapla-Myers, J., Gascon, F., Obaidul Haque, M., Kaewmanee, M., Leigh, L., Markham, B.L., 2018. Sentinel-2A MSI and Landsat-8 OLI radiometric cross comparison over desert sites. Eur. J. Remote Sens. 51 (1), 822–837.
Baumann, M., Ozdogan, M., Richardson, A.D., Radeloff, V.C., 2017. Phenology from Landsat when data is scarce: using MODIS and dynamic time-warping to combine multi-year Landsat imagery to derive annual phenology curves. Int. J. Appl. Earth Obs. Geoinf. 54, 72–83.
Beamer, J.P., Huntington, J.L., Morton, C.G., Pohll, G.M., 2013. Estimating annual groundwater evapotranspiration from phreatophytes in the great basin using Landsat and flux tower measurements. J. Am. Water Resour. Assoc. 49 (3), 518–533.
Belward, A.S., Skøien, J.O., 2015. Who launched what, when and why; trends in global land-cover observation capacity from civilian earth observation satellites. ISPRS J. Photogramm. Remote Sens. 103, 115–128.
Betts, R.A., 2000. Offset of the potential carbon sink from boreal forestation by decreases in surface albedo. Nature. 408 (6809), 187.
Bhandari, S., Phinn, S., Gill, T., 2012. Preparing Landsat Image Time Series (LITS) for monitoring changes in vegetation phenology in Queensland, Australia. Remote Sens. 4 (6), 1856–1886.
Bhardwaj, A., Joshi, P.K., Sam, L., Singh, M.K., Singh, S., Kumar, R., 2015. Applicability of Landsat 8 data for characterizing glacier facies and supraglacial debris. Int. J. Appl. Earth Obs. Geoinf. 38, 51–64.
Bindschadler, R., 2003. Tracking subpixel-scale sastrugi with advanced land imager. IEEE Trans. Geosci. Remote Sens. 41 (6), 1373–1377.
Bolton, D.K., White, J.C., Wulder, M.A., Coops, N.C., 2018. Updating stand-level forest inventories using airborne laser scanning and Landsat time series data. Int. J. Appl. Earth Obs. Geoinf. 66, 174–183.
Braaten, J., Cohen, W.B., Yang, Z., 2015. Automated cloud and cloud shadow identification in Landsat MSS imagery for temperate ecosystems. Remote Sens. Environ. 169, 128–138.
Broich, M., Huete, A., Paget, M., Ma, X., Tulbure, M., Coupe, N.R., Evans, B., Beringer, J., Devadas, R., Davies, K., Held, A., 2015. A spatially explicit land surface phenology data product for science, monitoring and natural resources management applications. Environ. Model Softw. 64, 191–204.
Brooks, E.B., Thomas, V.A., Wynne, R.H., Coulston, J.W., 2012. Fitting the multitemporal curve: a Fourier series approach to the missing data problem in remote sensing analysis. IEEE Trans. Geosci. Remote Sens. 50, 3340–3353.
Brooks, E.B., Wynne, R.H., Thomas, V.A., Blinn, C.E., Coulston, J.W., 2014. On-the-fly massively multitemporal change detection using statistical quality control charts and Landsat data. IEEE Trans. Geosci. Remote Sens. 52 (6), 3316–3332.
Burkhalter, J.P., Martin, T.C., Allen, R.G., Kjaersgaard, J., Wilson, E., Alvarado, R., Polly, J.S., 2013. Estimating crop water use via remote sensing techniques vs. conventional methods in the South Platte River Basin, Colorado. J. Am. Water Resour. Assoc. 49 (3), 498–517.
Butchart, S.H., Walpole, M., Collen, B., Van Strien, A., Scharlemann, J.P., Almond, R.E., Baillie, J.E., Bomhard, B., Brown, C., Bruno, J., Carpenter, K.E., 2010. Global biodiversity: indicators of recent declines. Science. 328 (5982), 1164–1168.
Butler, D., 2014. Many eyes on earth. Nature. 505 (7482), 143–144.
Campagnolo, M.L., Sun, Q., Liu, Y., Schaaf, C.B., Wang, Z., Román, M.O., 2016. Estimating the effective spatial resolution of the operational BRDF, albedo, and nadir reflectance products from MODIS and VIIRS. Remote Sens. Environ. 175, 52–64.
Chander, G., Markham, B.L., Helder, D.L., 2009. Summary of current radiometric calibration coefficients for Landsat MSS, TM, ETM+, and EO-1 ALI sensors. Remote Sens. Environ. 113, 893–903.
Choi, H., Bindschadler, R., 2004. Cloud detection in Landsat imagery of ice sheets using shadow matching technique and automatic normalized difference snow index threshold value decision. Remote Sens. Environ. 91, 237–242.
Chu, T., Guo, X., Takeda, K., 2016. Remote sensing approach to detect post-fire vegetation regrowth in Siberian boreal larch forest. Ecol. Indic. 62, 32–46.
Claverie, M., Vermote, E.F., Franch, B., Masek, J.G., 2015. Evaluation of the Landsat-5 TM and Landsat-7 ETM + surface reflectance products. Remote Sens. Environ. 169, 390–403.
Claverie, M., Ju, J., Masek, J.G., Dungan, J.L., Vermote, E.F., Roger, J.-C., Skakun, S.V., Justice, C., 2018. The harmonized Landsat and Sentinel-2 surface reflectance data set. Remote Sens. Environ. 219, 145–161.
Cohen, W.B., Yang, Z., Kennedy, R., 2010. Detecting trends in forest disturbance and recovery using yearly Landsat time series: 2. TimeSync—tools for calibration and validation. Remote Sens. Environ. 114 (12), 2911–2924.
Cohen, W.B., Yang, Z., Stehman, S.V., Schroeder, T.A., Bell, D.M., Masek, J.G., Huang, C., Meigs, G.W., 2016. Forest disturbance across the conterminous United States from 1985–2012: the emerging dominance of forest decline. For. Ecol. Manag. 360, 242–252.
Cohen, W.B., Healey, S.P., Yang, Z., Stehman, S.V., Brewer, C.K., Brooks, E.B., Gorelick, N., Huang, C., Hughes, M.J., Kennedy, R.E., Loveland, T.R., Moisen, G.G., Schroeder, T.A., Vogelmann, J.E., Woodcock, C.E., Yang, L., Zhu, Z., 2017. How similar are forest disturbance maps derived from different Landsat time series algorithms? Forests. 8 (4), 98.
Concha, J.A., Schott, J.R., 2016. Retrieval of color producing agents in case 2 waters using Landsat 8. Remote Sens. Environ. 185, 95–107.
Cook, M., Schott, J.R., Mandel, J., Raqueno, N., 2014. Development of an operational calibration methodology for the Landsat thermal data archive and initial testing of the atmospheric compensation component of a land surface temperature (LST) product from the archive. Remote Sens. 6 (11), 11244–11266.
Crawford, C.J., 2015. MODIS Terra collection 6 fractional snow cover validation in mountainous terrain during spring snowmelt using Landsat TM and ETM+. Hydrol. Process. 29, 128–138.
Crawford, C.J., Manson, S.M., Bauer, M.E., Hall, D.K., 2013. Multitemporal snow cover mapping in mountainous terrain for Landsat climate data record development. Remote Sens. Environ. 135, 224–233.
Cui, Z., Montanaro, M., Gerace, A., Schott, J.R., Markham, B., 2015. Requirement sensitivity studies for a future Landsat sensor. In: Earth Observing Systems XX. Vol. 9607. International Society for Optics and Photonics, pp. 96070S.
de la Fuente-Sáiz, D., Ortega-Farías, S., Fonseca, D., Ortega-Salazar, S., Kilic, A., Allen, R., 2017. Calibration of METRIC model to estimate energy balance over a drip-irrigated apple orchard. Remote Sens. 9 (7), 670.
De Sy, V., Herold, M., Achard, F., Asner, G.P., Held, A., Kellndorfer, J., Verbesselt, J., 2012. Synergies of multiple remote sensing data sources for REDD+ monitoring. Curr. Opin. Environ. Sustain. 4 (6), 696–706.
Dechoz, C., Poulain, V., Massera, S., Languille, F., Greslou, D., de Lussy, F., Gaudel, A., L'Helguen, C., Picard, C., Trémas, T., 2015. Sentinel 2 global reference image. In: Image and Signal Processing for Remote Sensing XXI. vol. 9643. International Society for Optics and Photonics, pp. 96430A.
DeVries, B., Decuyper, M., Verbesselt, J., Zeileis, A., Herold, M., Joseph, S., 2015. Tracking disturbance-regrowth dynamics in tropical forests using structural change detection and Landsat time series. Remote Sens. Environ. 169, 320–334.
Dolman, A.J., Belward, A.S., Briggs, S., Dowell, M., Eggleston, S., Hill, K., Richter, C., Simmons, A., 2016. A post-Paris look at climate observations. Nat. Geosci. 9 (9), 646.
Doxani, G., Vermote, E., Roger, J.C., Gascon, F., Adriaensen, S., Frantz, D., Hagolle, O., Hollstein, A., Kirches, G., Li, F., Louis, J., Mangin, A., Pahlevan, N., Pflug, B., Vanhellemont, Q., 2018. Atmospheric correction inter-comparison exercise. Remote Sens. 10 (2), 352.
Dozier, J., 1989. Spectral signature of alpine snow cover from the Landsat Thematic Mapper. Remote Sens. Environ. 28, 9–22.
Drusch, M., Del Bello, U., Carlier, S., Colin, O., Fernandez, V., Gascon, F., Hoersch, B., Isola, C., Laberinti, P., Martimort, P., Meygret, A., Spoto, F., Sya, O., Marchese, F., Bargellini, P., 2012. Sentinel-2: ESA's optical high-resolution mission for GMES operational services. Remote Sens. Environ. 120, 25–36.
Dwyer, J., Roy, D., Sauer, B., Jenkerson, C., Zhang, H., Lymburner, L., 2018. Analysis ready data: enabling analysis of the Landsat archive. Remote Sens. 10 (9), 1363.
Fahnestock, M., Scambos, T., Moon, T., Gardner, A., Haran, T., Klinger, M., 2016. Rapid large-area mapping of ice flow using Landsat 8. Remote Sens. Environ. 185, 84–94.
Feng, M., Sexton, J.O., Channan, S., Townshend, J.R., 2016. A global, high-resolution (30-m) inland water body dataset for 2000: first results of a topographic–spectral classification algorithm. Int. J. Digital Earth 9 (2), 113–133.
Finer, M., Novoa, S., Weisse, M.J., Petersen, R., Mascaro, J., Souto, T., Stearns, F., Martinez, R.G., 2018. Combating deforestation: from satellite to intervention. Science. 360 (6395), 1303–1305.
Fisher, J.I., Mustard, J.F., Vadeboncoeur, M.A., 2006. Green leaf phenology at Landsat resolution: scaling from the field to the satellite. Remote Sens. Environ. 100, 265–279.
Fisher, J.B., Melton, F.S., Middleton, E.M., Hain, C.R., Anderson, M.C., Allen, R.G., McCabe, M.F., Hook, S., Baldocchi, D.D., Townsend, P.A., Kilic, A., Tu, K., Miralles, D.D., Perret, J., Lagouarde, J.-P., Waliser, D., Purdy, A.J., French, A.N., Schimel, D., Famiglietti, J.S., Stephens, G., Wood, E.F., 2017. The future of evapotranspiration: global requirements for ecosystem functioning, carbon and climate feedbacks, agricultural management, and water resources. Water Resour. Res. 53 (4), 2618–2626.
Flood, N., 2013. Seasonal composite Landsat TM/ETM plus images using the Medoid (a multi-dimensional median). Remote Sens. 5, 6481–6500.
Fogt, R.L., Scambos, T.A., 2014. Antarctica. In: State of the Climate in 2013. 95(7). Bulletin of the American Meteorological Society, Boston, pp. S143. http://pal.lternet.edu/docs/bibliography/Public/509lterc.pdf (accessed: Jan 10, 2019).
Frantz, D., Röder, A., Stellmes, M., Hill, J., 2017. Phenology-adaptive pixel-based compositing using optical earth observation imagery. Remote Sens. Environ. 190, 331–347.
Franz, B.A., Bailey, S.W., Kuring, N., Werdell, P.J., 2015. Ocean color measurements with the operational land imager on Landsat-8: implementation and evaluation in SeaDAS. J. Appl. Remote. Sens. 9, 096070.
Frazier, R.J., Coops, N.C., Wulder, M.A., 2015. Boreal shield forest disturbance and recovery trends using Landsat time series. Remote Sens. Environ. 170, 317–327.
Frazier, R.J., Coops, N.C., Wulder, M.A., Hermosilla, T., White, J.C., 2018. Analyzing spatial and temporal variability in short-term rates of post-fire vegetation return from Landsat Time Series. Remote Sens. Environ. 205, 32–45.

Gallo, K., Stensaas, G., Dwyer, J., Longhenry, R., 2017. A land product characterization system for comparative analysis of satellite data and products. Remote Sens. 10 (1), 48.
Gao, F., Masek, J., Schwaller, M., Hall, F., 2006. On the blending of the Landsat and MODIS surface reflectance: predict daily Landsat surface reflectance. IEEE Trans. Geosci. Remote Sens. 44 (8), 2207–2218.
Gao, F., Hilker, T., Zhu, X., Anderson, M., Masek, J., Wang, P., Yang, Y., 2015. Fusing Landsat and MODIS data for vegetation monitoring. IEEE Geosci. Remote Sens. Mag. 3 (3), 47–60.
Gao, F., Anderson, M., Zhang, X., Yang, Z., Alfieri, J., Kustas, W., Mueller, R., Johnson, D., Prueger, J., 2017. Toward mapping crop progress at field scales through fusion of Landsat and MODIS imagery. Remote Sens. Environ. 188, 9–25.
Gao, F., Anderson, M.C., Daughtry, C., Johnson, D., 2018. Assessing the variability of corn and soybean yields in central Iowa using high spatiotemporal resolution multi-satellite imagery. Remote Sens. 10, 1489.
Gardner, A.S., Moholdt, G., Scambos, T., Fahnstock, M., Ligtenberg, S., van den Broeke, M. Nilsson, J., 2018. Increased West Antarctic and unchanged East Antarctic ice discharge over the last 7 years. Cryosphere 12 (2), 521–547.
Gascon, F., Bouzinac, C., Thépaut, O., Jung, M., Francesconi, B., Louis, J., Lonjou, V., Lafrance, B., Massera, S., Gaudel-Vacaresse, A., Languille, F., 2017. Copernicus sentinel-2A calibration and products validation status. Remote Sens. 9 (6), 584.
GCOS, 2016. The Global Observing System for Climate: Implementation Needs. 200 World Meteorological Organisation, Geneva 341 p.. Available at: https://library.wmo.int/doc_num.php?explnum_id=3417, Accessed date: 10 January 2019.
Gerace, A.D., Schott, J.R., Nevins, R., 2013. Increased potential to monitor water quality in the near-shore environment with Landsat's next-generation satellite. J. Appl. Remote. Sens. 7 (1), 073558.
GOFC-GOLD, 2016. A Sourcebook of Methods and Procedures for Monitoring and Reporting Anthropogenic Greenhouse Gas Emissions and Removals Associated with Deforestation, Gains and Losses of Carbon Stocks in Forests Remaining Forests, and Forestation. GOFC-GOLD Report Version COP22-1. GOFC-GOLD Land Cover Project Office, Wageningen University, The Netherlands Available at: http://www.gofcgold.wur.nl/redd/, Accessed date: 10 January 2019.
Gómez, C., Wulder, M.A., White, J.C., Montes, F., Delgado, J.A., 2012. Characterizing 25 years of change in the area, distribution, and carbon stock of Mediterranean pines in Central Spain. Int. J. Remote Sens. 33, 5546–5573.
Gómez, C., White, J.C., Wulder, M.A., 2016. Time-series informed land cover: a review. Int. J. Photogramm. Remote Sens. 116, 55–72.
Goodwin, N.R., Coops, N.C., Wulder, M.A., Gillanders, S., Schroeder, T.A., Nelson, T., 2008. Estimation of insect infestation dynamics using a temporal sequence of Landsat data. Remote Sens. Environ. 112, 3680–3689.
Goodwin, N.R., Magnussen, S., Coops, N.C., Wulder, M.A., 2010. Curve fitting of time-series Landsat imagery for characterizing a mountain pine beetle infestation. Int. J. Remote Sens. 31, 3263–3271.
Gordon, H.R., 1997. Atmospheric correction of ocean color imagery in the Earth Observing System era. J. Geophys. Res.-Atmos. 102 (D14), 17081–17106.
Gordon, H.R., Wang, M., 1994. Retrieval of water-leaving radiance and aerosol optical thickness over the oceans with SeaWiFS: a preliminary algorithm. Appl. Opt. 33, 443–452.
Gorelick, N., Hancher, M., Dixon, M., Ilyushchenko, S., Thau, D., Moore, R., 2017. Google Earth Engine: planetary-scale geospatial analysis for everyone. Remote Sens. Environ. 202, 18–27.
Goward, S., Arvidson, T., Williams, D., Faundeen, J., Irons, J., Franks, S., 2006. Historical record of Landsat global coverage. Photogramm. Eng. Remote Sens. 72 (10), 1155–1169.
Goward, S.N., Williams, D.L., Arvidson, T., Rocchio, L.E., Irons, J.R., Russell, C.A., Johnston, S.S., 2017. Landsat's Enduring Legacy: Pioneering Global Land Observations from Space. American Society for Photogrammetry and Remote Sensing, Bethesda, MD (586 p).
Griffiths, P., van der Linden, S., Kuemmerle, T., Hostert, P., 2013a. A pixel-based Landsat compositing algorithm for large area land cover mapping. IEEE J. Sel. Top. Appl. Earth Obs. Remote Sens. 6 (5), 2088–2101.
Griffiths, P., Müller, D., Kuemmerle, T., Hostert, P., 2013b. Agricultural land change in the Carpathian ecoregion after the breakdown of socialism and expansion of the European Union. Environ. Res. Lett. 8, 045024.
Griffiths, P., Kuemmerle, T., Baumann, M., Radeloff, V.C., Abrudan, I.V., Lieskovsky, J., Munteanu, C., Ostapowicz, K., Hostert, P., 2014. Forest disturbances, forest recovery, and changes in forest types across the Carpathian ecoregion from 1985 to 2010 based on Landsat image composites. Remote Sens. Environ. 151, 72–88.
Griffiths, P., Jakimow, B., Hostert, P., 2018. Reconstructing long term annual deforestation dynamics in Pará and Mato Grosso using the Landsat archive. Remote Sens. Environ. 216, 497–513.
Gutman, G., Huang, C., Chander, G., Noojipady, P., Masek, J.G., 2013. Assessment of the NASA–USGS global land survey (GLS) datasets. Remote Sens. Environ. 134, 249–265.
Hall, D.K., Ormsby, J.P., Bindschadler, R.A., Siddalingaiah, H., 1987. Characterization of snow and ice reflectance zones on glaciers using Landsat Thematic Mapper data. Ann. Glaciol. 9 (1), 104–108.
Hall, D.K., Crawford, C.J., DiGirolamo, N.E., Riggs, G.A., Foster, J.L., 2015. Detection of earlier snowmelt in the Wind River range, Wyoming, using Landsat imagery, 1972–2013. Remote Sens. Environ. 162, 45–54.
Hansen, M.C., Potapov, P.V., Moore, R., Hancher, M., Turubanova, S.A., Tyukavina, A., Thau, D., Stehman, S.V., Goetz, S.J., Loveland, T.R., Kommareddy, A., Egorov, A., Chini, L., Justice, C.O., Townshend, J.R.G., 2013. High-resolution global maps of 21st-century forest cover change. Science 342, 850–853.
Hansen, M.C., Egorov, A., Potapov, P.V., Stehman, S.V., Tyukavina, A., Turubanova, S.A., Roy, D.P., Goetz, S.J., Loveland, T.R., Ju, J., Kommareddy, A., Kovalskyy, V., Forsyth, C., Bents, T., 2014. Monitoring conterminous United States (CONUS) land cover change with web-enabled Landsat data (WELD). Remote Sens. Environ. 140, 466–484.
Hawbaker, T.J., Vanderhoof, M.K., Beal, Y.J., Takacs, J.D., Schmidt, G.L., Falgout, J.T., Williams, B., Fairaux, N.M., Caldwell, M.K., Picotte, J.J., Howard, S.M., 2017. Mapping burned areas using dense time-series of Landsat data. Remote Sens. Environ. 198, 504–522.
Healey, S.P., Cohen, W.B., Yang, Z., Brewer, C.K., Brooks, E.B., Gorelick, N., Hernandez, A.J., Huang, C., Hughes, M.J., Kennedy, R.E., Loveland, T.R., 2018. Mapping forest change using stacked generalization: an ensemble approach. Remote Sens. Environ. 204, 717–728.
Hedley, J.D., Roelfsema, C., Brando, V., Giardino, C., Kutser, T., Phinn, S., Mumby, P.J., Barrilero, O., Laporte, J., Koetz, B., 2018. Coral reef applications of Sentinel-2: coverage, characteristics, bathymetry and benthic mapping with comparison to Landsat 8. Remote Sens. Environ. 216, 598–614.
Helder, D., Markham, B., Morfitt, R., Storey, J., Barsi, J., Gascon, F., Clerc, S., LaFrance, B., Masek, J., Roy, D., 2018. Observations and recommendations for the calibration of Landsat 8 OLI and sentinel 2 MSI for improved data interoperability. Remote Sens. 10, 1340.
Hendrickx, J.M., Allen, R.G., Brower, A., Byrd, A.R., Hong, S.H., Ogden, F.L., Pradhan, N.R., Robison, C.W., Toll, D., Trezza, R., Umstot, T.G., 2016. Benchmarking optical/thermal satellite imagery for estimating evapotranspiration and soil moisture in decision support tools. JAWRA J. Am. Water Resour. Assoc. 52 (1), 89–119.
Hermosilla, T., Wulder, M.A., White, J.C., Coops, N.C., Hobart, G.W., 2015a. An integrated Landsat time series protocol for change detection and generation of annual gap free surface reflectance composites. Remote Sens. Environ. 158, 220–234.
Hermosilla, T., Wulder, M.A., White, J.C., Coops, N.C., Hobart, G.W., 2015b. Regional detection, characterization, and attribution of annual forest change from 1984 to 2012 using Landsat-derived time-series metrics. Remote Sens. Environ. 170, 121–132.
Hermosilla, T., Wulder, M.A., White, J.C., Coops, N.C., Hobart, G.W., Campbell, L.B., 2016. Mass data processing of time series Landsat imagery: pixels to data products for forest monitoring. Int. J. Digital Earth 9, 1035–1054.
Hermosilla, T., Wulder, M.A., White, J.C., Coops, N.C., Hobart, G.W., 2018. Disturbance-informed annual land cover classification maps of Canada's forested ecosystems for a 29-year Landsat time series. Can. J. Remote. Sens. 44 (1), 67–87.
Hermosilla, T., Wulder, M.A., White, J.C., Coops, N.C., Pickell, P.D., Bolton, D.K., 2019. Impact of time on interpretations of forest fragmentation: three-decades of fragmentation dynamics over Canada. Remote Sens. Environ. 222, 65–77.
Holden, C.E., Woodcock, C.E., 2016. An analysis of Landsat 7 and Landsat 8 underflight data and the implications for time series investigations. Remote Sens. Environ. 185, 16–36.
Hostert, P., Roder, A., Hill, J., 2003. Coupling spectral unmixing and trend analysis for monitoring of long-term vegetation dynamics in Mediterranean rangelands. Remote Sens. Environ. 87, 183–197.
Huang, C., Goward, S.N., Masek, J.G., Thomas, N., Zhu, Z., Vogelmann, J.E., 2010. An automated approach for reconstructing recent forest disturbance history using dense Landsat time series stacks. Remote Sens. Environ. 114, 183–198.
Hughes, M.J., Kaylor, S.D., Hayes, D.J., 2017. Patch-based forest change detection from Landsat time series. Forests 8 (5), 166.
Hulley, G.C., Hook, S.J., 2009. The north American ASTER land surface emissivity database (NAALSED) version 2.0. Remote Sens. Environ. 113 (9), 1967–1975.
Hulley, G.C., Hughes, C.G., Hook, S.J., 2012. Quantifying uncertainties in land surface temperature and emissivity retrievals from ASTER and MODIS thermal infrared data. J. Geophys. Res.-Atmos. 117 (D23).
Huntington, J., McGwire, K., Morton, C., Snyder, K., Peterson, S., Erickson, T., Niswonger, R., Carroll, R., Smith, G., Allen, R., 2016. Assessing the role of climate and resource management on groundwater dependent ecosystem changes in arid environments with the Landsat archive. Remote Sens. Environ. 185, 186–197.
Huntington, J.L., Hegewisch, K.C., Daudert, B., Morton, C.G., Abatzoglou, J.T., McEvoy, D.J., Erickson, T., 2017. Climate engine: cloud computing and visualization of climate and remote sensing data for advanced natural resource monitoring and process understanding. Bull. Am. Meteorol. Soc. 98 (11), 2397–2410.
Hurni, K., Schneider, A., Heinimann, A., Nong, D.H., Fox, J., 2017. Mapping the expansion of boom crops in mainland southeast Asia using dense time stacks of Landsat data. Remote Sens. 9 (4), 320.
Irons, J.R., Dwyer, J.L., Barsi, J.A., 2012. The next Landsat satellite: the Landsat data continuity mission. Remote Sens. Environ. 122, 11–21.
Jeong, S., Howat, I.M., 2015. Performance of Landsat 8 operational land imager for mapping ice sheet velocity. Remote Sens. Environ. 170, 90–101.
Ju, J., Roy, D.P., Vermote, E., Masek, J., Kovalskyy, V., 2012. Continental-scale validation of MODIS-based and LEDAPS Landsat ETM+ atmospheric correction methods. Remote Sens. Environ. 122, 175–184.
Justice, C.O., Vermote, E., Townshend, J.R., Defries, R., Roy, D.P., Hall, D.K., Salomonson, V.V., Privette, J.L., Riggs, G., Strahler, A., Lucht, W., 1998. The moderate resolution imaging spectroradiometer (MODIS): land remote sensing for global change research. IEEE Trans. Geosci. Remote Sens. 36 (4), 1228–1249.
Kalma, J.D., McVicar, T.R., McCabe, M.F., 2008. Estimating land surface evaporation: a review of methods using remotely sensed surface temperature data. Surv. Geophys. 29 (4–5), 421–469.
Kampe, T.U., Good, W.S., 2017. Pathway to future sustainable land imaging: the compact hyperspectral prism spectrometer. In: Earth Observing Systems XXII. Vol. 10402 International Society for Optics and Photonics 1040208.
Karimi, P., Bastiaanssen, W.G.M., Molden, D., 2013. Water accounting plus (WA+) - a water accounting procedure for complex river basins based on satellite measurements. Hydrol. Earth Syst. Sci. 17, 2459–2472.

Keeling, C.D., Whorf, T.P., 2005. Atmospheric Carbon Dioxide Record From Mauna Loa. Carbon Dioxide Research Group, Scripps Institution of Oceanography, University of California, La Jolla, California 92093-0444. https://cdiac.ess-dive.lbl.gov/trends/co2/sio-mlo.html (Accessed Jan 11, 2019).
Keenan, R.J., Reams, G.A., Achard, F., de Freitas, J.V., Grainger, A., Lindquist, E., 2015. Dynamics of global forest area: results from the FAO global Forest resources assessment 2015. For. Ecol. Manag. 352, 9–20.
Kennedy, R.E., Yang, Z., Cohen, W.B., 2010. Detecting trends in forest disturbance and recovery using yearly Landsat time series: 1. LandTrendr - Temporal segmentation algorithms. Remote Sens. Environ. 114, 2897–2910.
Kennedy, R.E., Yang, Z., Cohen, W.B., Pfaff, E., Braaten, J., Nelson, P., 2012. Spatial and temporal patterns of forest disturbance and regrowth within the area of the Northwest Forest Plan. Remote Sens. Environ. 122, 117–133.
Kennedy, R.E., Andréfouët, S., Cohen, W.B., Gómez, C., Griffiths, P., Hais, M., Healey, S.P., Helmer, E.H., Hostert, P., Lyons, M.B., Meigs, G.W., 2014. Bringing an ecological view of change to Landsat-based remote sensing. Front. Ecol. Environ. 12 (6), 339–346.
Kennedy, R.E., Yang, Z., Braaten, J., Copass, C., Antonova, N., Jordan, C., Nelson, P., 2015. Attribution of disturbance change agent from Landsat time series in support of habitat monitoring in the Puget Sound region, USA. Remote Sens. Environ. 166, 271–285.
Kingslake, J., Ely, J.C., Das, I., Bell, R.E., 2017. Widespread movement of meltwater onto and across Antarctic ice shelves. Nature 544 (7650), 349–352.
Klein, A.G., Hall, D.K., Riggs, G.A., 1998. Improving snow cover mapping in forests through the use of a canopy reflectance model. Hydrol. Process. 12, 1723–1744.
Kloiber, S.M., Brezonik, P.L., Olmanson, L.G., Bauer, M.E., 2002. A procedure for regional lake water clarity assessment using Landsat multispectral data. Remote Sens. Environ. 82 (1), 38–47.
Kustas, W.P., Anderson, M.C., Alfieri, J.G., Knipper, K., Torres-Rua, A., Parry, C.K., Nieto, H., Agam, N., White, A., Gao, F., McKee, L., Prueger, J.H., Hipps, L.E., Los, S.O., Alsina, M., Sanchez, L., Sams, B., Dokoozlian, N., McKee, M., Jones, S., McElrone, A., Heitman, J.L., Howard, A.M., Post, K., Melton, F.S., Hain, C., 2018. The grape remote sensing atmospheric profile and evapotranspiration eXperiment (GRAPEX). Bull. Am. Meteorol. Soc. https://doi.org/10.1175/BAMS-D-16-0244.1. (Accessed Jan 10, 2019).
Laraby, K., Schott, J.R., 2018. Uncertainty estimation method and Landsat 7 global validation for the Landsat surface temperature product. Remote Sens. Environ. 216, 472–481.
Lawrence, R., Ripple, W.J., 1999. Calculating change curves for multitemporal satellite imagery: Mount St. Helens 1980-1995. Remote Sens. Environ. 67, 309–319.
Leslie, C.R., Serbina, L.O., Miller, H.M., 2017. Landsat and agriculture—case studies on the uses and benefits of Landsat imagery in agricultural monitoring and production. U.S. Geol. Surv. Open File Rep. 2017–1034https://doi.org/10.3133/ofr20171034. (accessed: Jan 10, 2019. 27 p).
Lewis, A., Oliver, S., Lymburner, L., Evans, B., Wyborn, L., Mueller, N., Raevksi, G., Hooke, J., Woodcock, R., Sixsmith, J., Wu, W., 2017. The Australian geoscience data cube—foundations and lessons learned. Remote Sens. Environ. 202, 276–292.
Li, J., Roy, D.P., 2017. A global analysis of sentinel-2A, sentinel-2B and Landsat-8 data revisit intervals and implications for terrestrial monitoring. Remote Sens. 9 (9), 902.
Loveland, T.R., Dwyer, J.L., 2012. Landsat: building a strong future. Remote Sens. Environ. 122, 22–29.
Loveland, T.R., Irons, J.R., 2016. Landsat 8: the plans, the reality, and the legacy. Remote Sens. Environ. 185, 1–6.
Lucht, W., Schaaf, C.B., Strahler, A.H., 2000. An algorithm for the retrieval of albedo from space using semiempirical BRDF models. IEEE Trans. Geosci. Remote Sens. 38 (2), 977–998.
Lymburner, L., Botha, E., Hestir, E., Anstee, J., Sagar, S., Dekker, A., Malthus, T., 2016. Landsat 8: providing continuity and increased precision for measuring multi-decadal time series of total suspended matter. Remote Sens. Environ. 185, 108–118.
Madoui, A., Gauthier, S., Leduc, A., Bergeron, Y., Valeria, O., 2015. Monitoring forest recovery following wildfire and harvest in boreal forests using satellite imagery. Forests 6, 4105–4134.
Malakar, N.K., Hulley, G.C., Hook, S.J., Laraby, K., Cook, M., Schott, J.R., 2018. An operational land surface temperature product for Landsat thermal data: methodology and validation. IEEE Trans. Geosci. Remote Sens. 99, 1–19.
Mankoff, K.D., Jacobs, S.S., Tulaczyk, S.M., Stammerjohn, S.E., 2012. The role of Pine Island Glacier ice shelf basal channels in deep-water upwelling, polynyas and ocean circulation in Pine Island Bay, Antarctica. Ann. Glaciol. 53 (60), 123–128.
Markham, B.L., Helder, D.L., 2012. Forty-year calibrated record of earth-reflected radiance from Landsat: a review. Remote Sens. Environ. 122, 30–40.
Markham, B., Barsi, J., Kvaran, G., Ong, L., Kaita, E., Biggar, S., Czapla-Myers, J., Mishra, N., Helder, D., 2014. Landsat-8 operational land imager radiometric calibration and stability. Remote Sens. 6 (12), 12275–12808.
Masek, J.G., Vermote, E.F., Saleous, N.E., Wolfe, R., Hall, F.G., Huemmrich, K.F., Gao, F., Kutler, J., Lim, T.K., 2006. A Landsat surface reflectance dataset for North America, 1990-2000. IEEE Geosci. Remote Sens. Lett. 3, 68–72.
Masek, J.G., Goward, S.N., Kennedy, R.E., Cohen, W.B., Moisen, G.G., Schleeweis, K., Huang, C., 2013. United States forest disturbance trends observed using Landsat time series. Ecosystems. 16, 1086–1104.
McDowell, N.G., Coops, N.C., Beck, P.S., Chambers, J.Q., Gangodagamage, C., Hicke, J.A., Huang, C.Y., Kennedy, R.E., Krofcheck, D.J., Litvak, M., Meddens, A.J., 2015. Global satellite monitoring of climate-induced vegetation disturbances. Trends Plant Sci. 20 (2), 114–123.
Meigs, G.W., Kennedy, R.E., Cohen, W.B., 2011. A Landsat time series approach to characterize bark beetle and defoliator impacts on tree mortality and surface fuels in conifer forests. Remote Sens. Environ. 115, 3707–3718.
Melaas, E.K., Friedl, M.A., Zhu, Z., 2013. Detecting interannual variation in deciduous broadleaf forest phenology using Landsat TM/ETM + data. Remote Sens. Environ. 132, 176–185.
Melaas, E.K., Sulla-Menashe, D., Gray, J.M., Black, T.A., Morin, T.H., Richardson, A.D., Friedl, M.A., 2016. Multisite analysis of land surface phenology in North American temperate and boreal deciduous forests from Landsat. Remote Sens. Environ. 186, 452–464.
Melton, F.S., Johnson, L.F., Lund, C.P., Pierce, L.L., Michaelis, A.R., Hiatt, S.H., Guzman, A., Adhikari, D.D., Purdy, A.J., Rosevelt, C., Votava, P., 2012. Satellite irrigation management support with the terrestrial observation and prediction system: a framework for integration of satellite and surface observations to support improvements in agricultural water resource management. IEEE J. Sel. Top. Appl. Earth Obs. Remote Sens. 5 (6), 1709–1721.
Mesinger, F., DiMego, G., Kalnay, E., Mitchell, K., Shafran, P.C., Ebisuzaki, W., Jović, D., Woollen, J., Rogers, E., Berbery, E.H., Ek, M.B., 2006. North American regional reanalysis. Bull. Am. Meteorol. Soc. 87 (3), 343–360.
Mihailovic, D.T., Kapor, D., Hogrefe, C., Lazic, J., Tosic, T., 2004. Parameterization of albedo over heterogeneous surfaces in coupled land-atmosphere schemes for environmental modeling. Part I: theoretical background. Environ. Fluid Mech. 4 (1), 57–77.
Miles, K.E., Willis, I.C., Benedek, C.L., Williamson, A.G., Tedesco, M., 2017. Toward monitoring surface and subsurface lakes on the Greenland ice sheet using Sentinel-1 SAR and Landsat-8 OLI imagery. Front. Earth Sci. 5, 58.
Mishra, N., Haque, M.O., Leigh, L., Aaron, D., Helder, D., Markham, B., 2014. Radiometric cross calibration of Landsat 8 operational land imager (OLI) and Landsat 7 enhanced thematic mapper plus (ETM+). Remote Sens. 6 (12), 12619–12638.
Moisen, G.G., Meyer, M.C., Schroeder, T.A., Liao, X., Schleeweis, K.G., Freeman, E.A., Toney, C., 2016. Shape selection in Landsat time series: a tool for monitoring forest dynamics. Glob. Chang. Biol. 22, 3518–3528.
Montanaro, M., Gerace, A., Lunsford, A., Reuter, D., 2014. Stray light artifacts in imagery from the Landsat 8 thermal infrared sensor. Remote Sens. 6 (11), 10435–10456.
Montanaro, M., Gerace, A., Rohrbach, S., 2015. Toward an operational stray light correction for the Landsat 8 thermal infrared sensor. Appl. Opt. 54 (13), 3963–3978.
Morfitt, R., Barsi, J., Levy, R., Markham, B., Micijevic, E., Ong, L., Scaramuzza, P., Vanderwerff, K., 2015. Landsat-8 operational land imager (OLI) radiometric performance on-orbit. Remote Sens. 7 (2), 2208–2237.
Mouginot, J., Rignot, E., Scheuchl, B., Millan, R., 2017. Comprehensive annual ice sheet velocity mapping using Landsat-8, Sentinel-1, and RADARSAT-2 data. Remote Sens. 9 (4), 1–20.
Mueller, N., Lewis, A., Roberts, D., Ring, S., Melrose, R., Sixsmith, J., Lymburner, L., McIntyre, A., Tan, P., Curnow, S., Ip, A., 2016. Water observations from space: mapping surface water from 25 years of Landsat imagery across Australia. Remote Sens. Environ. 174, 341–352.
National Academies of Sciences, Engineering, and Medicine, 2018. Thriving on our Changing Planet: A Decadal Strategy for Earth Observation from Space. The National Academies Press, Washington, DC. https://doi.org/10.17226/24938. (Accessed: Jan 10, 2019).
Nechad, B., Ruddick, K., Park, Y., 2010. Calibration and validation of a generic multisensor algorithm for mapping of total suspended matter in turbid waters. Remote Sens. Environ. 114, 854–866.
Nelson, K.J., Steinwand, D., 2015. A Landsat data tiling and compositing approach optimized for change detection in the conterminous United States. Photogramm. Eng. Remote. Sens. 81, 573–586.
Nijland, W., Bolton, D.K., Coops, N.C., Stenhouse, G., 2016. Imaging phenology; scaling from camera plots to landscapes. Remote Sens. Environ. 177, 13–20.
NRC, National Research Council, 2013. Landsat and beyond: Sustaining and enhancing the nation's land imaging program. The National Academies Press, Washington, DC, pp. 73. https://www.nap.edu/catalog/18420/landsat-and-beyond-sustaining-and-enhancing-the-nations-land-imaging.
Oeser, J., Pflugmacher, D., Senf, C., Heurich, M., Hostert, P., 2017. Using intra-annual Landsat time series for attributing forest disturbance agents in Central Europe. Forests 8 (7), 251.
Orheim, O., Lucchitta, B.K., 1987. Snow and ice studies by thematic mapper and multispectral scanner Landsat images. Ann. Glaciol. 9 (1), 109–118.
Orheim, O., Lucchitta, B.K., 1988. Numerical analysis of Landsat thematic mapper images of Antarctica: surface temperatures and physical properties. Ann. Glaciol. 11, 109–120.
Otkin, J.A., Anderson, M.C., Hain, C., Svoboda, M., Johnson, D., Mueller, R., Tadesse, T., Wardlow, B., Brown, J., 2016. Assessing the evolution of soil moisture and vegetation conditions during the 2012 United States flash drought. Agric. For. Meteorol. 218, 230–242.
Pahlevan, N., Schott, J.R., 2013. Leveraging EO-1 to evaluate capability of new generation of Landsat sensors for coastal/inland water studies. IEEE J. Sel. Top. Appl. Earth Obs. Remote Sens. 6 (2), 360–374.
Pahlevan, N., Lee, Z., Hu, C., Schott, J.R., 2014a. Diurnal remote sensing of coastal/oceanic waters: a radiometric analysis for geostationary coastal and air pollution events. Appl. Opt. 53, 648–665.
Pahlevan, N., Lee, Z., Wei, J., Schaff, C., Schott, J., Berk, A., 2014b. On-orbit radiometric characterization of OLI (Landsat-8) for applications in aquatic remote sensing. Remote Sens. Environ. 154, 272–284.
Pahlevan, N., Sheldon, P., Peri, F., Wei, J., Shang, Z., Sun, Q., Chen, R.F., Lee, Z., Schaaf, C.B., Schott, J.R., 2016. Calibration/validation of Landsat-Derived Ocean Colour Products in Boston Harbour. In: ISPRS - International Archives of the Photogrammetry. Remote Sensing and Spatial Information Sciencespp. 1165–1168.
Pahlevan, N., Schott, J.R., Franz, B.A., Zibordi, G., Markham, B., Bailey, S., Schaaf, C.B., Ondrusek, M., Greb, S., Strait, C.M., 2017. Landsat 8 remote sensing reflectance (R rs)

products: evaluations, intercomparisons, and enhancements. Remote Sens. Environ. 190, 289–301.
Pahlevan, N., Balasubramanian, S., Sarkar, S., Franz, B., 2018. Toward long-term aquatic science products from heritage Landsat missions. Remote Sens. 10 (9), 1337.
Pasquarella, V.J., Holden, C.E., Kaufman, L., Woodcock, C.E., 2016. From imagery to ecology: leveraging time series of all available Landsat observations to map and monitor ecosystem state and dynamics. In: Remote Sensing in Ecology and Conservation. 2(3). pp. 152–170.
Pasquarella, V.J., Bradley, B.A., Woodcock, C.E., 2017. Near-real-time monitoring of insect defoliation using Landsat time series. Forests. 8 (8), 275.
Pekel, J.F., Cottam, A., Gorelick, N., Belward, A.S., 2016. High-resolution mapping of global surface water and its long-term changes. Nature 540 (7633), 418–422.
Pereira, H.M., Ferrier, S., Walters, M., Geller, G.N., Jongman, R.H.G., Scholes, R.J., Bruford, M.W., Brummitt, N., Butchart, S.H.M., Cardoso, A.C., Coops, N.C., 2013. Essential biodiversity variables. Science 339 (6117), 277–278.
Pettorelli, N., Wegmann, M., Skidmore, A., Mücher, S., Dawson, T.P., Fernandez, M., Lucas, R., Schaepman, M.E., Wang, T., O'Connor, B., Jongman, R.H., 2016. Framing the concept of satellite remote sensing essential biodiversity variables: challenges and future directions. In: Remote Sensing in Ecology and Conservation. 2(3). pp. 122–131.
Pflugmacher, D., Cohen, W.B., Kennedy, R.E., 2012. Using Landsat-derived disturbance history (1972–2010) to predict current forest structure. Remote Sens. Environ. 172, 146–165.
Pflugmacher, D., Cohen, W.B., Kennedy, R.E., Yang, Z., 2014. Using Landsat-derived disturbance and recovery history and Lidar to map forest biomass dynamics. Remote Sens. Environ. 151, 124–137.
Pickell, P.D., Hermosilla, T., Frazier, R.J., Coops, N.C., Wulder, M.A., 2015. Forest recovery trends derived from Landsat time series for North American boreal forests. Int. J. Remote Sens. 37 (1), 138–149.
Pope, A., Scambos, T.A., Moussavi, M., Tedesco, M., Willis, M., Shean, D., Grigsby, S., 2016. Estimating supraglacial lake depth in West Greenland using Landsat 8 and comparison with other multispectral methods. Cryosphere 10, 15.
Potapov, P.V., Turubanova, S., Hansen, M.C., 2011. Regional-scale boreal forest cover and change mapping using Landsat data composites for European Russia. Remote Sens. Environ. 115, 548–561.
Potapov, P.V., Turubanova, S.A., Tyukavina, A., Krylov, A.M., McCarty, J.L., Radeloff, V.C., Hansen, M.C., 2015. Eastern Europe's forest cover dynamics from 1985 to 2012 quantified from the full Landsat archive. Remote Sens. Environ. 159, 28–43.
Reuter, D., Richardson, C., Pellerano, F., Irons, J., Allen, R., Anderson, M., Jhabvala, M., Lunsford, A., Montanaro, M., Smith, R., Tesfaye, Z., 2015. The Thermal Infrared Sensor (TIRS) on Landsat 8: Design overview and pre-launch characterization. Remote Sens. 7 (1), 1135–1153.
Reynolds, J.F., Smith, D.M.S., Lambin, E.F., Turner, B.L., Mortimore, M., Batterbury, S.P., Downing, T.E., Dowlatabadi, H., Fernandez, R.J., Herrick, J.E., Huber-Sannwald, E., Jiang, H., Leemans, R., Lynam, T., Maestre, M.T., Ayarza, M., Walker, B., 2007. Global desertification: building a science for dryland development. Science 316 (5826), 847–851.
Rienecker, M.M., Suarez, M.J., Gelaro, R., Todling, R., Bacmeister, J., Liu, E., Bosilovich, M.G., Schubert, S.D., Takacs, L., Kim, G.K., Bloom, S., 2011. MERRA: NASA's modern-era retrospective analysis for research and applications. J. Clim. 24 (14), 3624–3648.
Rittger, K., Painter, T.H., Dozier, J., 2013. Assessment of methods for mapping snow cover from MODIS. Adv. Water Resour. 51, 367–380.
Rosenthal, W., Dozier, J., 1996. Automated mapping of montane snow cover at subpixel resolution from the Landsat thematic mapper. Water Resour. Res. 32, 115–130.
Roy, D.P., Yan, L., 2018. Robust Landsat-based crop time series modelling. Remote Sens. Environ. doi:https://doi.org/10.1016/j.rse.2018.06.038 (Accessed: Jan 10, 2019).
Roy, D.P., Borak, J.S., Devadiga, S., Wolfe, R.E., Zheng, M., Descloitres, J., 2002. The MODIS land product quality assessment approach. Remote Sens. Environ. 83 (1–2), 62–76.
Roy, D.P., Ju, J., Kline, K., Scaramuzza, P.L., Kovalskyy, V., Hansen, M., Loveland, T.R., Vermote, E., Zhang, C., 2010. Web-enabled Landsat data (WELD): Landsat ETM+ composited mosaics of the conterminous United States. Remote Sens. Environ. 114, 35–49.
Roy, D.P., Wulder, M.A., Loveland, T.R., W. C.E, Allen, R.G., Anderson, M.C., Helder, D., Irons, J.R., Johnson, D.M., Kennedy, R., Scambos, T.A., Schaaf, C.B., Schott, J.R., Sheng, Y., Vermote, E.F., Belward, A.S., Bindschadler, R., Cohen, W.B., Gao, F., Hipple, J.D., Hostert, P., Huntington, J., Justice, C.O., Kilic, A., Kovalskyy, V., Lee, Z.P., Lymburner, L., Masek, J.G., McCorkel, J., Shuai, Y., Trezza, R., Vogelmann, J., Wynne, R.H., Zhu, Z., 2014. Landsat-8: science and product vision for terrestrial global change research. Remote Sens. Environ. 145, 154–172.
Roy, D., Zhang, H., Ju, J., Gomez-Dans, J., Lewis, P., Schaaf, C., Sun, Q., Li, J., Huang, H., Kovalskyy, V., 2016a. A general method to normalize Landsat reflectance data to nadir BRDF adjusted reflectance. Remote Sens. Environ. 176, 255–271.
Roy, D.P., Kovalskyy, V., Zhang, H.K., Vermote, E.F., Yan, L., Kumar, S.S., Egorov, A., 2016b. Characterization of Landsat-7 to Landsat-8 reflective wavelength and normalized difference vegetation index continuity. Remote Sens. Environ. 185, 57–70.
Roy, D.P., Li, J., Zhang, H.K., Yan, L., Huang, H., Li, Z., 2017. Examination of Sentinel-2A multi-spectral instrument (MSI) reflectance anisotropy and the suitability of a general method to normalize MSI reflectance to nadir BRDF adjusted reflectance. Remote Sens. Environ. 199, 25–38.
Sakamoto, T., Wardlow, B.D., Gitelson, A.A., 2011. Detecting spatiotemporal changes of corn developmental stages in the US Corn Belt using MODIS WDRVI data. IEEE Trans. Geosci. Remote Sens. 49, 1926–1936.
Scambos, T.A., Dutkiewicz, M.J., Wilson, J.C., Bindschadler, R.A., 1992. Application of image cross-correlation to the measurement of glacier velocity using satellite image data. Remote Sens. Environ. 42 (3), 177–186.
Scambos, T.A., Campbell, G.G., Pope, A., Haran, T., Muto, A., Lazzara, M., Reijmer, C.H., van den Broeke, M.R., 2018. Ultralow surface temperatures in East Antarctica from satellite thermal infrared mapping: the coldest places on Earth. Geophys. Res. Lett. 45 (12), 6124–6133.
Schaaf, C.B., Gao, F., Strahler, A.H., Lucht, W., Li, X., Tsang, T., Strugnell, N.C., Zhang, X., Jin, Y., Muller, J.P., Lewis, P., 2002. First operational BRDF, albedo nadir reflectance products from MODIS. Remote Sens. Environ. 83 (1–2), 135–148.
Schaeffer, B.A., Iiames, J., Dwyer, J., Urquhart, E., Salls, W., Rover, J., Seegers, B., 2018. An initial validation of Landsat 5 and 7 derived surface water temperature for US lakes, reservoirs, and estuaries. Int. J. Remote Sens. https://doi.org/10.1080/01431161.2018.1471545.
Schingler Jr., R.H., 2015. Perspectives on Public - Private Partnerships in U.S. Earth Observing Programs. Joint Hearing of the Subcommittees for Space and Environemtn of the House Science Committee 10 p. http://docs.house.gov/meetings/SY/SY16/20151117/104181/HHRG-114-SY16-Wstate-SchinglerR-20151117.pdf, Accessed date: 10 January 2019.
Schmidt, G., Jenkerson, C., Masek, J., Vermote, E., Gao, F., 2013. Landsat ecosystem disturbance adaptive processing system (LEDAPS) algorithm description. In: U.S. Geological Survey Open-File Report 2013. U.S. Geological Survey 17 p.. https://pubs.usgs.gov/of/2013/1057/ofr13_1057.pdf, Accessed date: 10 January 2019.
Schneider, A., 2012. Monitoring land cover change in urban and pen-urban areas using dense time stacks of Landsat satellite data and a data mining approach. Remote Sens. Environ. 124, 689–704.
Schott, J.R., Hook, S.J., Barsi, J.A., Markham, B.L., Miller, J., Padula, F.P., Raqueno, N.G., 2012. Thermal infrared radiometric calibration of the entire Landsat 4, 5, and 7 archive (1982–2010). Remote Sens. Environ. 122, 41–49.
Schott, J.R., Gerace, A., Raqueno, N., Ientilucci, E., Raqueno, R., Lunsford, A.W., 2014. Chasing the TIRS ghosts: calibrating the Landsat 8 thermal bands. In: SPIE Optical Engineering + Applications. International Society for Optics and Photonics, pp. 92181A.
Schott, J.R., Gerace, A., Woodcock, C.E., Wang, S., Zhu, Z., Wynne, R.H., Blinn, C.E., 2016. The impact of improved signal-to-noise ratios on algorithm performance: case studies for Landsat class instruments. Remote Sens. Environ. 185, 37–45.
Schroeder, T.A., Wulder, M.A., Healey, S.P., Moisen, G.G., 2011. Mapping wildfire and clearcut harvest disturbances in boreal forests with Landsat time series data. Remote Sens. Environ. 115, 1421–1433.
Schroeder, T.A., Schleeweis, K.G., Moisen, G.G., Toney, C., Cohen, W.B., Freeman, E.A., Yang, Z., Huang, C., 2017. Testing a Landsat-based approach for mapping disturbance causality in U.S. forests. Remote Sens. Environ. 195, 230–243.
Schwieder, M., Leitão, P.J., da Cunha Bustamante, M.M., Ferreira, L.G., Rabe, A., Hostert, P., 2016. Mapping Brazilian savanna vegetation gradients with Landsat time series. Int. J. Appl. Earth Obs. Geoinf. 52, 361–370.
Selkowitz, D.J., Forster, R.R., 2016. Automated mapping of persistent ice and snow cover across the western US with Landsat. ISPRS J. Photogramm. Remote Sens. 117, 126–140.
Senf, C., Pflugmacher, D., Wulder, M.A., Hostert, P., 2015. Characterizing spectral-temporal patterns of defoliator and bark beetle disturbances using Landsat time series. Remote Sens. Environ. 170, 166–177.
Senf, C., Pflugmacher, D., Heurich, M., Krueger, T., 2017a. A Bayesian hierarchical model for estimating spatial and temporal variation in vegetation phenology from Landsat time series. Remote Sens. Environ. 194, 155–160.
Senf, C., Seidl, R., Hostert, P., 2017b. Remote sensing of forest insect disturbances: current state and future directions. Int. J. Appl. Earth Obs. Geoinf. 60, 49–60.
Sheng, Y., Song, C., Wang, J., Lyons, E.A., Knox, B.R., Cox, J.S., Gao, F., 2016. Representative lake water extent mapping at continental scales using multi-temporal Landsat-8 imagery. Remote Sens. Environ. 185, 129–141.
Shuai, Y., Masek, J.G., Gao, F., Schaaf, C.B., 2011. An algorithm for the retrieval of 30-m snow-free albedo from Landsat surface reflectance and MODIS BRDF. Remote Sens. Environ. 115 (9), 2204–2216.
Skakun, S., Roger, J.C., Vermote, E.F., Masek, J.G., Justice, C.O., 2017. Automatic sub-pixel co-registration of Landsat-8 operational land imager and sentinel-2A multi-spectral instrument images using phase correlation and machine learning based mapping. Int. J. Digital Earth 10 (12), 1253–1269.
Sommer, S., Zucca, C., Grainger, A., Cherlet, M., Zougmore, R., Sokona, Y., Hill, J., Della Peruta, R., Roehrig, J., Wang, G., 2011. Application of indicator systems for monitoring and assessment of desertification from national to global scales. Land Degrad. Dev. 22 (2), 184–197.
Song, C., Woodcock, C.E., Seto, K.C., Lenney, M.P., Macomber, S.A., 2001. Classification and change detection using Landsat TM data: when and how to correct atmospheric effects? Remote Sens. Environ. 75 (2), 230–244.
Steffen, K., Schweiger, A., 1991. NASA team algorithm for sea ice concentration retrieval from defense meteorological satellite program special sensor microwave imager: comparison with Landsat satellite imagery. J. Geophys. Res. Oceans 96 (C12), 21971–21987.
Storey, J., Choate, M., Lee, K., 2014. Landsat 8 operational land imager on-orbit geometric calibration and performance. Remote Sens. 6, 11127–11152.
Storey, J., Roy, D.P., Masek, J., Gascon, F., Dwyer, J., Choate, M., 2016. A note on the temporary mis-registration of Landsat-8 operational land imager (OLI) and Sentinel-2 multi spectral instrument (MSI) imagery. Remote Sens. Environ. 186, 121–122.
Strauss, M., 2017. Flotilla of Tiny Satellites Will Photograph the Entire Earth every Day. Science. http://www.sciencemag.org/news/2017/02/flotilla-tiny-satellites-will-photograph-entire-earth-every-day, Accessed date: 11 January 2019.
Sun, L., Gao, F., Anderson, M., Kustas, W.P., Alsina, M., Sanchez, L., Sams, Brent, McKee, L.G., Dulaney, W.P., White, A., Alfieri, J.G., Prueger, J.H., Melton, F., Post, K., 2017. Daily mapping of 30m LAI and NDVI for grape yield prediction in California vineyards. Remote Sens. 9, 317.

Swithinbank, C., 1988. Satellite image atlas of glaciers of the world: Antarctica. In: Williams, R.S., Ferrigno, J.G. (Eds.), U.S. Geological Survey Professional Paper 1386-B.
Torbick, N., Huang, X., Ziniti, B., Johnson, D., Masek, J., Reba, M., 2018. Fusion of moderate resolution earth observations for operational crop type mapping. Remote Sens. 10, 1058.
Tulbure, M.G., Broich, M., Stehman, S.V., Kommareddy, A., 2016. Surface water extent dynamics from three decades of seasonally continuous Landsat time series at subcontinental scale in a semi-arid region. Remote Sens. Environ. 178, 142–157.
UN, 2015. United Nations, Transforming our World: The 2030 Agenda for Sustainable Development, UN A/RES/70/1. (41 p).
UNCCD, 2013. Decision 22/COP.11 Advice on How Best to Measure Progress on Strategic Objectives 1, 2 and 3 of The Strategy ICCD/COP(11)/23/Add.1.
UNDESA, 2017. United Nations Department of Economic and Social Affairs, Population Division. World Population Prospects: The 2017 Revision, Key Findings and Advance Tables. Working Paper No. ESA/P/WP/248.
UNESC, 2017. United Nations Economic and Social Council Report of the Inter-agency and Expert Group on Sustainable Development Goal Indicators, E/CN.3/2017/2. pp. 49.
Vancutsem, C., Pekel, J.F., Bogaert, P., Defourny, P., 2007. Mean compositing, an alternative strategy for producing temporal syntheses. Concepts and performance assessment for SPOT VEGETATION time series. Int. J. Remote Sens. 28, 5123–5141.
Vermote, E.F., Tanré, D., Deuze, J.L., Herman, M., Morcette, J.J., 1997. Second simulation of the satellite signal in the solar spectrum, 6S: an overview. IEEE Trans. Geosci. Remote Sens. 35 (3), 675–686.
Vermote, E.F., El Saleous, N.Z., Justice, C.O., 2002. Atmospheric correction of MODIS data in the visible to middle infrared: first results. Remote Sens. Environ. 83 (1), 97–111.
Vermote, E., Justice, C., Claverie, M., Franch, B., 2016. Preliminary analysis of the performance of the Landsat 8/OLI land surface reflectance product. Remote Sens. Environ. 185, 46–56.
Verpoorter, C., Kutser, T., Seekell, D.A., Tranvik, L.J., 2014. A global inventory of lakes based on high-resolution satellite imagery. Geophys. Res. Lett. 41 (18), 6396–6402.
Vogeler, J.C., Braaten, J.D., Sesak, R.A., Falkowski, M.J., 2018. Extracting the full value of the Landsat archive: inter-sensor harmonization for the mapping of Minnesota forest canopy cover (1973–2015). Remote Sens. Environ. 209, 363–374.
Vogelmann, J.E., Xian, G., Homer, C., Tolk, B., 2012. Monitoring gradual ecosystem change using Landsat time series data analyses: case studies in selected forest and rangeland ecosystems. Remote Sens. Environ. 122, 92–105.
Vuolo, F., Ng, W.-T., Atzberger, C., 2017. Smoothing and gap-filling of high resolution multi-spectral time series: example of Landsat data. Int. J. Appl. Earth Obs. Geoinf. 57, 202–213.
Wang, Z., Schaaf, C.B., Strahler, A.H., Chopping, M.J., Román, M.O., Shuai, Y., Woodcock, C.E., Hollinger, D.Y., Fitzjarrald, D.R., 2014. Evaluation of MODIS albedo product (MCD43A) over grassland, agriculture and forest surface types during dormant and snow-covered periods. Remote Sens. Environ. 140, 60–77.
Wang, Z., Erb, A.M., Schaaf, C.B., Sun, Q., Liu, Y., Yang, Y., Shuai, Y., Casey, K.A., Román, M.O., 2016. Early spring post-fire snow albedo dynamics in high latitude boreal forests using Landsat-8 OLI data. Remote Sens. Environ. 185, 71–83.
Wei, J., Lee, Z., Garcia, R., Zoffoli, L., Armstrong, R.A., Shang, Z., Sheldon, P., Chen, R.F., 2018. An assessment of Landsat-8 atmospheric correction schemes and remote sensing reflectance products in coral reefs and coastal turbid waters. Remote Sens. Environ. 215, 18–32.
White, E., Roy, D.P., 2015. A contemporary decennial examination of changing agricultural field sizes using Landsat time series data. Geogr. Environ. 2, 33–54.
White, J.C., Gómez, C., Wulder, M.A., Coops, N.C., 2010. Characterizing temperate forest structural and spectral diversity with Hyperion EO-1 data. Remote Sens. Environ. 114 (7), 1576–1589.
White, J.C., Wulder, M.A., Gómez, C., Stenhouse, G., 2011. A history of habitat dynamics: characterizing 35 years of stand-replacing disturbance. Can. J. Remote. Sens. 37, 234–251.
White, J.C., Wulder, M.A., Hobart, G.W., Luther, J.E., Hermosilla, T., Griffiths, P., Coops, N.C., Hall, R.J., Hostert, P., Dyk, A., Guindon, L., 2014. Pixel-based image compositing for large-area dense time series applications and science. Can. J. Remote. Sens. 40, 192–212.
White, J.C., Wulder, M.A., Hermosilla, T., Coops, N.C., Hobart, G.W., 2017. A nationwide annual characterization of 25 years of forest disturbance and recovery for Canada using Landsat time series. Remote Sens. Environ. 194, 303–321.
White, J.C., Saarinen, N., Kankare, V., Wulder, M.A., Hermosilla, T., Coops, N.C., Pickell, P., Holopainen, M., Hyyppä, J., Vastaranta, M., 2018. Confirmation of post-harvest spectral recovery from Landsat time series using measures of forest cover and height derived from airborne laser scanning data. Remote Sens. Environ. 216, 262–275.
Willardson, A.G., 2014. Landsat thermal infrared imagery and western water management. J. Contemp. Water Res. Educ. 153 (1), 42–48.
Williams Jr.R.S., Ferrigno, J.G. (Eds.), 2010. Glaciers of Asia: U.S. Geological Survey Professional Paper 1386–F, pp. 349.
Williams, C.A., Gu, H., MacLean, R., Masek, J.G., Collatz, G.J., 2016. Disturbance and the carbon balance of US forests: a quantitative review of impacts from harvests, fires, insects, and droughts. Glob. Planet. Chang. 143, 66–80.
Woodcock, C.E., Allen, R., Anderson, M., Belward, A., Bindschadler, R., Cohen, W., Gao, F., Goward, S.N., Helder, D., Helmer, E., Nemani, R., Oreopoulos, L., Schott, J., Thenkabail, P.S., Vermote, E.F., Vogelmann, J., Wulder, M.A., Wynne, R., 2008. Free access to Landsat imagery. Science 302 (5879), 1011.
Wulder, M.A., White, J.C., Goward, S.N., Masek, J.G., Irons, J.R., Herold, M., Cohen, W.B., Loveland, T.R., Woodcock, C.E., 2008. Landsat continuity: issues and opportunities for land cover monitoring. Remote Sens. Environ. 112 (3), 955–969.
Wulder, M.A., Masek, J.G., Cohen, W.B., Loveland, T.R., Woodcock, C.E., 2012. Opening the archive: how free data has enabled the science and monitoring promise of Landsat. Remote Sens. Environ. 122, 2–10.
Wulder, M.A., Hilker, T., White, J.C., Coops, N.C., Masek, J.G., Pflugmacher, D., Crevier, Y., 2015. Virtual constellations for global terrestrial monitoring. Remote Sens. Environ. 170, 62–76.
Wulder, M.A., White, J.C., Loveland, T.R., Woodcock, C.E., Belward, A.S., Cohen, W.B., Fosnight, E.A., Shaw, J., Masek, J.G., Roy, D.P., 2016. The global Landsat archive: status, consolidation, and direction. Remote Sens. Environ. 185, 271–283.
Wulder, M.A., Coops, N.C., Roy, D.P., White, J.C., Hermosilla, T., 2018. Land cover 2.0. Int. J. Remote Sens. 39 (12), 4254–4284.
Yamazaki, D., Trigg, M.A., Ikeshima, D., 2015. Development of a global ~90 m water body map using multi-temporal Landsat images. Remote Sens. Environ. 171, 337–351.
Yan, L., Roy, D.P., 2014. Automated crop field extraction from multi-temporal web enabled Landsat data. Remote Sens. Environ. 144, 42–64.
Yan, L., Roy, D.P., 2016. Conterminous United States crop field size quantification from multi-temporal Landsat data. Remote Sens. Environ. 172, 67–86.
Yan, L., Roy, D.P., Zhang, H.K., Li, J., Huang, H., 2016. An automated approach for sub-pixel registration of Landsat-8 operational land imager (OLI) and Sentinel-2 multi spectral instrument (MSI) imagery. Remote Sens. 8 (6), 520.
Yang, Y., Anderson, M.C., Gao, F., Wardlow, B., Hain, C.R., Otkin, J.A., Yang, Y., Sun, L., Dulaney, W., 2018. Field-scale mapping of evaporative stress indicators of crop yield: an application over Mead, NE. Remote Sens. Environ. 210, 387–402.
Zeng, L., Wardlow, B.D., Wang, R., Shan, J., Tadesse, T., Hayes, M.J., Li, D., 2016. A hybrid approach for detecting corn and soybean phenology with time-series MODIS data. Remote Sens. Environ. 181, 237–250.
Zhang, X., Friedl, M.A., Schaaf, C.B., Strahler, A.H., Hodges, J.C.F., Gao, F., Reed, B.C., 2003. Monitoring vegetation phenology using MODIS. Remote Sens. Environ. 84 (3), 471–475.
Zhang, H.K., Roy, D.P., Yan, L., Li, Z., Huang, H., Vermote, E., Skakun, S., Roger, J.C., 2018. Characterization of Sentinel-2A and Landsat-8 top of atmosphere, surface, and nadir BRDF adjusted reflectance and NDVI differences. Remote Sens. Environ. 215, 482–494.
Zhe, Z., Wulder, M.A., Roy, D.P., Woodcock, C.E., Hansen, M.C., Radeloff, V.C., Healey, S.P., Schaaf, C., Hostert, P., Strobl, P., Pekel, J-F., Lymburner, L., Pahlevan, N., Scambos, T.A., 2019. Benefits of the Free and Open Landsat Data Policy. Remote Sens. Environ. https://doi.org/10.1016/j.rse.2019.02.016.
Zhu, Z., 2017. Change detection using Landsat time series: a review of frequencies, preprocessing, algorithms, and applications. ISPRS J. Photogramm. Remote Sens. 130, 370–384.
Zhu, Z., Woodcock, C.E., 2012. Object-based cloud and cloud shadow detection in Landsat imagery. Remote Sens. Environ. 118, 83–94.
Zhu, Z., Woodcock, C.E., 2014a. Continuous change detection and classification of land cover using all available Landsat data. Remote Sens. Environ. 144, 152–171.
Zhu, Z., Woodcock, C.E., 2014b. Automated cloud, cloud shadow, and snow detection in multitemporal Landsat data: an algorithm designed specifically for monitoring land cover change. Remote Sens. Environ. 152, 217–234.
Zhu, Z., Woodcock, C.E., Olofsson, P., 2012. Continuous monitoring of forest disturbance using all available Landsat imagery. Remote Sens. Environ. 122, 75–91.
Zhu, Z., Wang, S., Woodcock, C.E., 2015a. Improvement and expansion of the Fmask algorithm: cloud, cloud shadow, and snow detection for Landsats 4–7, 8, and Sentinel 2 images. Remote Sens. Environ. 159, 269–277.
Zhu, Z., Woodcock, C.E., Holden, C., Yang, Z., 2015b. Generating synthetic Landsat images based on all available Landsat data: predicting Landsat surface reflectance at any given time. Remote Sens. Environ. 162, 67–83.
Zhu, Z., Gallant, A.L., Woodcock, C.E., Pengra, B., Olofsson, P., Loveland, T.R., Jin, S., Dahal, D., Yang, L., Auch, R.F., 2016. Optimizing selection of training and auxiliary data for operational land cover classification for the LCMAP initiative. ISPRS J. Photogramm. Remote Sens. 122, 206–221.
Zhu, Z., Qiu, S., He, B., Deng, C., 2018. Cloud and cloud shadow detection for Landsat images: the fundamental basis for analyzing Landsat time series. In: Remote Sensing Time Series Image Processing. CRC Press, pp. 25–46.